Concept Study Report
概念検討書

SOLAR-C WG
Date 29, Jan, 2018, version 1

1. Science goals of the mission [1-1-1]
ミッションの意義

As a fundamental step towards answering how the plasma universe is created and evolves, and how the Sun influences the Earth and other planets in our solar system, the proposed mission is designed to comprehensively understand how mass and energy are transferred throughout the solar atmosphere. Understanding the solar atmosphere, which connects to the heliosphere via radiation, the solar wind and coronal mass ejections, and energetic particles is pivotal for establishing the conditions for life and habitability in the solar system.

2. Scientific objectives of the mission [1-2-1]
ミッションの科学目標

Solar-C_EUVST (EUV High-Throughput Spectroscopic Telescope) is a mission designed to provide a conclusive answer to the most fundamental question in solar physics: how does the interplay of magnetic fields and plasma drive solar activity (Figure 2.1)? The most significant examples of this interplay are atmospheric heating and explosive energy release, such as flares and coronal mass ejections (CMEs). Thus, the two primary science objectives for Solar-C_EUVST are:

I. Understand how fundamental processes lead to the formation of the solar atmosphere and the solar wind.
II. Understand how the solar atmosphere becomes unstable, releasing the energy that drives solar flares and eruptions.

To achieve these science objectives Solar-C_EUVST will

A. Seamlessly observe all the temperature regimes of the solar atmosphere from the chromosphere to the corona at the same time,
B. Resolve elemental structures of the solar atmosphere with high spatial resolution and cadence to track their evolution, and,
C. Obtain spectroscopic information on the dynamics of elementary processes taking place in the solar atmosphere.

Recent missions such as Hinode (Solar-B) have clearly demonstrated that different layers of the solar atmosphere are highly coupled with each other via magnetic fields (see Figure 2.2). This interplay happens at spatial and temporal scales that have not been resolved over the full range of temperature extremes 0.01 MK in the chromosphere to 1 MK in the corona to 10 MK in flares. To understand the physical interplay between the plasma and magnetic field, we must determine how mass and energy are transported, stored, and converted into other forms of energy in the solar atmosphere over vastly different physical domains.

Several recent missions have given a glimpse into what can be observed in the solar atmosphere at high spatial and temporal resolution. For example, during its 300 s rocket flight in 2012, the High Resolution Coronal Imager (Hi-C; Kobayashi et al. 2014) observed the solar corona at a resolution of 0.3-0.4" and a cadence of 5.5 s and was able to detect heating events that were largely invisible to lower resolution instruments (Testa et al. 2013). Furthermore, Hi-C also observed very narrow, braided field lines that appeared to be reconnecting and producing high-temperature plasma (Cirtain et al. 2013).

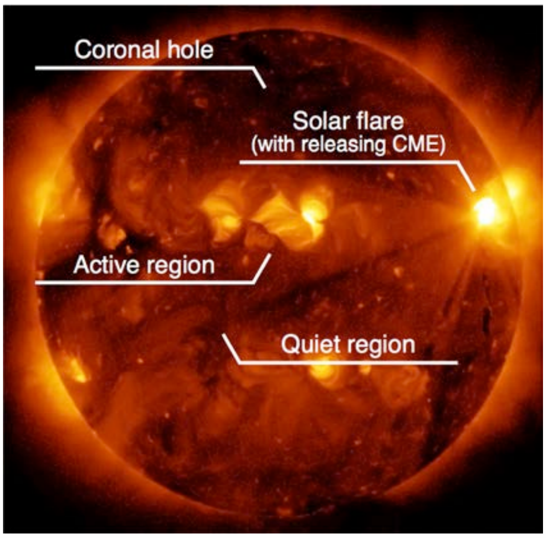

Figure 2.1: Solar coronal structures and activities in soft-Xray.

Finally, to truly understand the interplay of magnetic fields and plasma, simultaneous observations of the photosphere are essential. Several previous missions, such as SoHO, Hinode, and SDO (see section 3.3), have carried instruments to observe both the solar photosphere and the upper atmosphere. The latest generation of ground-based optical telescopes, however, represent a quantum leap over previous space-based instrumentation. Foremost among these observatories is the Daniel K. Inouye Solar Telescope (DKIST), which will have a diameter of 4 m and achieve an angular resolution as high as 0.03" or about 20 km on the solar surface. DKIST is nearing completion and is scheduled to become fully operational before the end of 2020. In 2027, the 4m European Solar Telescope (EST) is also planned to start observation, doubling the opportunity for coordinated observations of the magnetic field. To achieve the final link between the plasma dynamics and the magnetic field, Solar-C_EUVST observations will be coordinated with DKIST and other ground-based observatories located throughout the world.

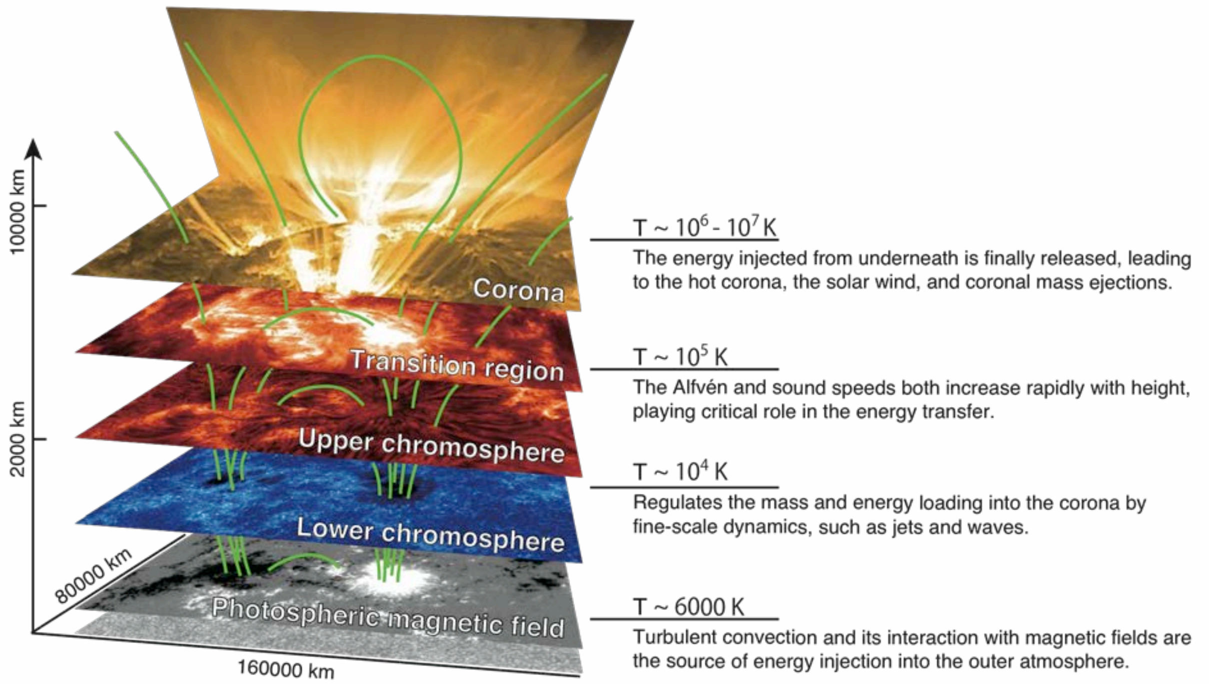

Figure 2.2: The layers of the solar atmosphere are coupled to each other by magnetic fields.

For the main scientific objectives we define sub-objectives (I-1~I-4, II-1~II-2) to be addressed with the Solar-C_EUVST mission. To tackle the sub-objectives, we also define the observing tasks at right side (labeled such as I-1-1) of Table 2.1, which describe what we want to observe with the mission. Details of the observing tasks are described in sections 3.2 and 5.1.

Table 2.1: Science objectives of the Solar-C_EUVST mission

<table>
<tr><td colspan="4">I. Understand How Fundamental Processes Lead to the Formation of the Solar Atmosphere and the Solar Wind</td></tr>
<tr><td colspan="4">Historically, two primary mechanisms have been proposed to explain how the chromosphere and corona are heated, namely small-scale magnetic reconnection and wave dissipation. Recently the role of small chromospheric jets called spicules has also been studied extensively. These mechanisms are also directly linked to the origin and acceleration of the solar wind. By investigating energy transfer and release on small spatial and temporal scales, Solar-C_EUVST will quantify the relative contributions of these mechanisms to the formation of the solar atmosphere and the solar wind.</td></tr>
<tr><td rowspan="5">I-1</td><td colspan="3">Quantify the Contribution of Nanoflares to Coronal Heating</td></tr>
<tr><td rowspan="4">Nanoflares, small-scale magnetic reconnection events, are a possible mechanism for heating the corona. Solar-C_EUVST will evaluate this hypothesis by observing high-temperature plasmas and their dynamical behavior through resolving elemental structures in the corona.</td><td>I-1-1</td><td>Measure the energy of small-scale heating events in the transition region and the corona in the energy range of $\sim 10^{24}$ - 10^{27} erg.</td></tr>
<tr><td>I-1-2</td><td>Observe intermittent processes that generate plasmas above 5 MK with high speed plasma motions.</td></tr>
<tr><td>I-1-3</td><td>Observe sub-arcsec braiding structures with high temporal and spatial resolutions.</td></tr>
<tr><td>I-1-4</td><td>Identify the driver of nanoflares by comparing spectroscopic diagnostics with simultaneous observations of the photosphere and low chromosphere.</td></tr>
<tr><td rowspan="4">I-2</td><td colspan="3">Quantify the Contribution of Wave Dissipation to Coronal Heating</td></tr>
<tr><td rowspan="3">The wave heating hypothesis suggests that waves propagate upwards from the solar surface and are dissipated, leading to the heating of the solar atmosphere. Solar-C_EUVST will quantify this scenario by measuring the characteristics of the waves at different heights and observing the thermalization process.</td><td>I-2-1</td><td>Detect Alfvén waves by measuring the propagation of fluctuations through different layers of the atmosphere.</td></tr>
<tr><td>I-2-2</td><td>Observe the thermalization process by measuring how transition region and coronal plasmas respond to the propagating waves.</td></tr>
<tr><td>I-2-3</td><td>Identify the source of upwardly propagating waves by comparing spectroscopic diagnostics with simultaneous observations of the photosphere and low chromosphere.</td></tr>
<tr><td rowspan="3">I-3</td><td colspan="3">Understand the Formation Mechanism of Spicules and Quantify Their Contribution to Coronal Heating</td></tr>
<tr><td rowspan="2">A spicule is a dynamic jet launched upwards from the lower atmosphere and is a fundamental ingredient of the solar chromosphere and the transition region. Solar-C_EUVST will clarify how spicules are created and quantify their mass and energy contribution to coronal heating.</td><td>I-3-1</td><td>Observe the thermal evolution of spicules (width ~0.4") from chromospheric to transition region and coronal temperatures. Quantify the mass flux that spicules supply to higher altitudes.</td></tr>
<tr><td>I-3-2</td><td>Identify the driving mechanisms of spicules by comparing spectroscopic diagnostics with simultaneous observations of the photosphere and low chromosphere.</td></tr>
</table>

I-4	**Understand the Source Regions and the Acceleration Mechanism of the Solar Wind**		
	The solar wind is the plasma flowing along open field lines into the heliosphere. This plasma is thought to be accelerated by Alfvén waves as it flows away from the solar surface. The wind originates in faint regions of the corona, making it difficult to measure the plasma properties. Solar-C_EUVST will provide sensitive measurements of the velocity, temperature, density, and abundance in these regions, revealing the formation and acceleration mechanisms of the solar wind.	I-4-1	Observe the velocity, temperature and density structures at the source regions of solar wind and clarify their relationship to the magnetic field structures.
		I-4-2	Detect signatures of coronal Alfvén waves in plume and inter-plume regions and measure their energy fluxes with height.
II. Understand How the Solar Atmosphere Becomes Unstable, Releasing the Energy that Drives Solar Flares and Eruptions			
Photospheric motions lead to the accumulation of free magnetic energy in the corona. This system eventually becomes unstable, releasing the energy through magnetic reconnection. This process of energy conversion heats the plasma to high temperatures and drives coronal mass ejections (CMEs). By measuring the properties of multi-temperature flaring plasma, Solar-C_EUVST will investigate why the reconnection is fast despite the high magnetic Reynolds number. It will also monitor the temporal evolution of solar active regions and identify the triggering mechanism for the flare and eruption.			
II-1	**Understand the Fast Magnetic Reconnection Process**		
	Magnetic reconnection is one of the fundamental processes for converting magnetic energy into the thermal and kinetic energy of the plasma. This process occurs much faster than is predicted by classical theory. Solar-C_EUVST will observe the dynamics of magnetic structures to understand the mechanisms that lead to fast magnetic reconnection in partially or fully ionized plasmas.	II-1-1	Probe plasma conditions and structures inside the reconnection region and clarify the role of shocks and magnetic islands in fast reconnection.
		II-1-2	Probe the conversion of energy by observing the chromospheric response to magnetic reconnection at very high cadence.
		II-1-3	Characterize the physical properties and dynamics of magnetic reconnection occurring in the chromosphere and transition region, where the plasma is different from the fully ionized plasma of the corona.
II-2	**Identify the Signatures of Global Energy Buildup and the Local Triggering of the Flare and Eruption**		
	Understanding the accumulation and release of free magnetic energy in the corona is a fundamental problem. Solar-C_EUVST will perform long-term monitoring of active regions to identify the signatures of energy buildup and high-resolution observations to understand the triggers of energy release.	II-2-1	Monitor long-term, large-scale evolution of active regions and identify the spectroscopic signatures of energy buildup.
		II-2-2	Characterize the dynamics of small-scale magnetic structures that trigger the eruption of flares and identify the MHD (magnetohydrodynamic) instability modes by comparing photospheric and low-chromospheric observations against numerical modeling.

3. Rationale for the scientific goals and objectives
ミッションの科学意義と目標の根拠

3.1. Scientific background, status of the relevant scientific area, etc.
科学的意義の根拠：研究の背景，当該分野の研究状況，等

There are two crucial facets of solar research that underline the scientific priority of Solar-C_EUVST. First, many of the phenomena that take place on the Sun also occur elsewhere in the universe. Therefore, the insights gained from Solar-C_EUVST will advance the knowledge of fundamental processes in astrophysical plasmas. Second, the Sun is the star that governs our space environment and, for a technologically advanced global society, this space environment is directly connected to our daily lives. Increasing our knowledge of solar variability is critical for humanity due to our ever-increasing reliance on space-based technologies for daily life. In this regard, there are several imperative scientific investigations, including understanding large-scale solar eruptions and the origin of the solar wind and its dynamics that directly affect our global environment and daily lives.

To reinforce the international support for this proposal, we would like to cite a study report on the future of solar physics for the decade of 2020 that was published by the Next Generation Solar Physics Mission (NGSPM)'s Science Objectives Team (SOT), an advisory team consisting of 14 scientists, chartered by the United States National Aeronautics and Space Administration (NASA), the Japan Aerospace Exploration Agency (JAXA), and the European Space Agency (ESA). The report (see Supplement A) lists scientific objectives in all the research areas related to solar physics and provides priorities for next generation solar physics missions to be realized in the mid 2020s. The report is based on extensive reviews of the broad interests of the heliophysics research community, following a public call for white papers in the fall of 2016 which resulted in 34 submissions describing science objectives, instruments and mission concepts, covering a wide variety of topics. Three top-level science objectives are identified: I) Formation mechanisms of the hot and dynamic outer solar atmosphere, II) Mechanisms of large-scale solar eruptions and foundations for predictions, and III) Mechanisms driving the solar cycle and irradiance variation. The Solar-C_EUVST mission aims to mainly cover topics I) and II) following a unique approach that is described in detail below.

I) Formation mechanisms of the hot and dynamic outer solar atmosphere

Hinode has revealed the dynamic behavior of small-scale magnetic field structures (~0.4") in the form of magnetic flux tubes at the photosphere. It is clear that the turbulent motions of the photosphere are responsible for the heating of the solar upper atmosphere. The mechanisms responsible for transporting energy up from the photosphere and dissipating it, however, are still not fully understood. Three plausible mechanisms, nanoflares, waves, and spicule heating, have been studied as possible solutions to the coronal heating problem. Furthermore, solar wind acceleration is also often discussed in the same framework.

Nanoflares: The photospheric motions lead to the twisting and braiding of the magnetic field (Figure 3.1-A) which permeates the solar atmosphere. Parker (1972) was among the first to recognize that the dissipation of this topological complexity through magnetic reconnection could heat the solar corona to high temperatures. Most previous spectroscopic instruments, however, have been unable to routinely follow small-scale heating events at the "nanoflare" size (10^{24}-10^{27} erg) envisioned in the Parker model (Winebarger et al. 2012, Ishikawa et al. 2014). Thus the detailed plasma properties of small-scale coronal heating events are largely unexplored.

Waves: The magnetized solar atmosphere is filled with a rich assortment of waves that are an important source of energy. Some of the oldest theories of coronal heating involve the dissipation of waves that are generated at low heights and propagate upward into the chromosphere and corona (e.g., Ionson 1978, Heyvaerts & Priest 1983). Imaging observations by SoHO/EIT identified that the coronal waves are the slow-mode MHD wave, but the total energy brought by this mode was not enough to heat the corona. Coronal Multi-Channel Polarimeter (CoMP, ground-based coronagraph) detected Alfvén waves in line-of-sight velocity images of the solar corona (Figure 3.1-B, Tomczyk et al. 2007). Hinode has detected Alfvén waves in the chromosphere (Okamoto et al. 2007). Models based on this concept, however, have a difficult time reproducing the observed temperatures in the corona unless the wave fluxes are much larger than are generally observed (e.g., van Ballegooijen et al. 2017). There have been no observations with seamless temperature coverage through the chromosphere to the corona as well as high temporal resolution.

Spicules: Previous instruments such as Hinode/SOT have clearly revealed that the chromosphere is dominated by a multitude of thin (average of 300 km or 0.4"), dynamical, jet-like extrusions called spicules (Figure 3.1-C, De Pontieu et al. 2007). Combined Hinode/SOT and IRIS observations have greatly advanced our understanding of spicule evolution over a wider range of temperatures. It appears that a subset of chromospheric spicules can be heated to coronal temperatures as they rise and supply hot mass to the corona or that a considerable amount of energy could be channeled into the corona by small-scale eruptions driven by photospheric vortices or cyclones (e.g., Wedemeyer-Böhm et al. 2012, Iijima & Yokoyama 2017). Existing spectroscopic observations at higher temperatures, however, do not have the spatial resolution or cadence to follow spicule evolution further and determine how much they contribute to the mass and energy budget of the corona. Even at low resolution, the measurements of asymmetric line profiles suggest that the contribution of spicules is important (De Pontieu et al. 2009).

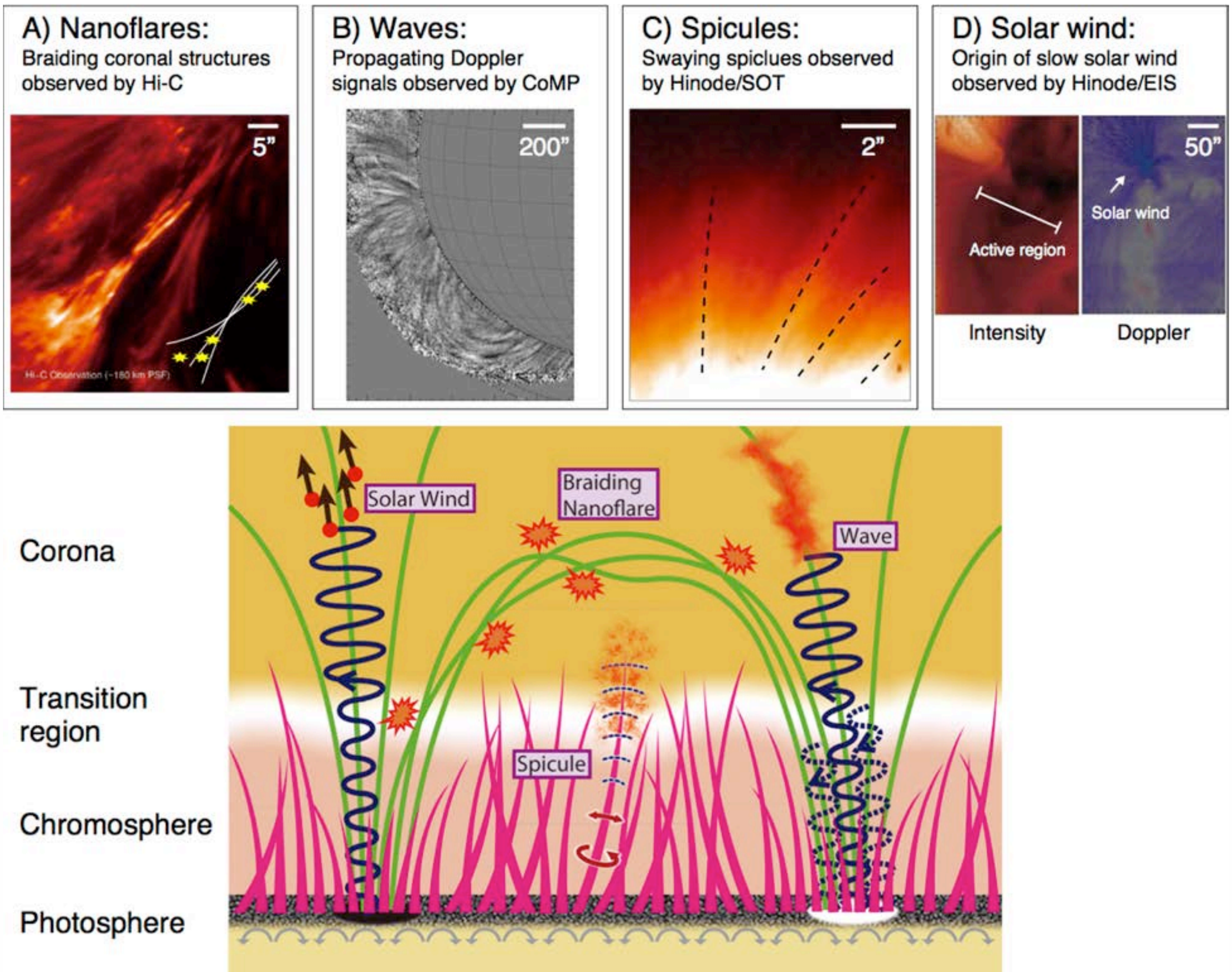

Figure 3.1: Cartoon of the formation mechanisms of the hot and dynamic outer solar atmosphere (bottom). A) nanoflare with braiding structure observed by the Hi-C rocket, B) propagating Alfvén wave observed by CoMP, C) spicules observed by Hinode/SOT, D) the origin of the slow solar wind at the edge of an active region observed by Hinode/EIS.

Solar wind: A significant fraction of the magnetic field on the Sun is open and extends into the heliosphere. Thus, some of the same processes that lead to the formation of high temperature loops in the closed corona heat and accelerate the solar wind. In situ observations show that the solar wind has, at least approximately, a bi-modal nature with fast (~800 km/s) and slow (<400 km/s) components (e.g., McComas et al. 1998). The fast wind is known to originate in the polar coronal holes. The origin of the slow wind, however, has not been fully established. Equatorial coronal holes, active region (AR) outflows (Figure 3.1-D, Harra et al. 2008), and streamers have all been proposed as sites for the slow solar wind. Furthermore, the mechanism for accelerating both fast and slow solar winds have not been identified. The height at which the solar wind acceleration begins is still controversial; some observations suggest lower heights (less than 1 solar radii, Hahn & Savin 2013) while theory and other observations suggest higher heights (larger than 2 solar radii, Gabriel et al. 2003, 2005). Because the solar wind acceleration region is very faint, new spectroscopic observations with high throughput are needed to detect signatures of Alfvén waves and measure energy fluxes with height.

II) Mechanisms of large-scale solar eruptions and foundations for predictions

It is now widely accepted that solar flares are caused by magnetic reconnection, the physical process that rearranges the magnetic configuration and converts magnetic energy into kinetic and thermal energies with non-thermal particle acceleration. While previous space missions have improved our understanding of flare reconnection, there still remain several key mechanisms that need to be resolved, especially those related to fast magnetic reconnection. As the strongest flares, and ones that affect Earth, often occur in the ARs, we focus on the large-scale evolution of ARs and the triggering process of flares. These studies are key for formulating flare prediction algorithms.

Solar flares: Solar flares represent the high-energy tail of the distribution of magnetic reconnection events and are therefore ideal for studying how magnetic energy is dissipated in the corona via reconnection. Although the Yohkoh, SoHO, TRACE, RHESSI, Hinode, SDO, and IRIS missions have led to a better understanding of solar flares, features such as inflows, high-velocity jets and shocks, which are thought to be central to the reconnection scenario, have not yet been observed systematically (Figure 3.2-A, Daughton et al. 2011). It has been proposed that these features must be too faint to observe as intensity features with current instrumentation (Figure 3.2-C). However, they should be visible as Doppler shifted features in spectra, while rapid heating at the location where shocks are observed should result in non-equilibrium ionization and different ion and electron temperatures. There have been some observations of these phenomena (e.g., Hara et al. 2011; Imada et al. 2013), but previous spectroscopic instruments have lacked the throughput needed to quickly scan large areas and routinely observe flares.

Fast magnetic reconnection: Standard magnetic reconnection theory (e.g., the Sweet-Parker reconnection model) predicts reconnection rate that is too slow to explain observed reconnection events in the solar corona. Several theoretical studies recently suggested that small magnetic islands in the reconnecting current sheet are important. The development of magnetic islands or plasmoids in the current sheets (e.g. Loureiro et al. 2007, see Figure 3.2-B) can lead to fast reconnection (e.g., Shibayama et al. 2015). To clarify the fast magnetic reconnection process, observing the reconnection region is essential. The temperature evolution of the reconnection region can be inferred by measuring the intensities of lines of highly ionized iron, e.g. from Fe XVIII through Fe XXIV (6 ~ 15 MK), while high velocity flows are expected in or close to the reconnection region. It is therefore crucial to determine the current sheet geometry and test the standard models. However, this can only be done using high cadence observations with high spectral resolution of the full group of hot Fe lines (Fe XII to XXIV: 1.5~15 MK) within and above the forming X-ray loops, which is difficult with existing spectrometers as they do not possess enough throughput.

AR evolution and flare triggers: As illustrated in Figure 3.2-D, solar flares occur as a result of a large-scale AR development, namely, the storage of free magnetic energy in the corona. In response to the photospheric evolution, the AR corona is known to show spectroscopic signatures such as upflows with non-thermal line broadening in the pre-flare phase (e.g. Hinode/EIS observations by Harra et al. 2009, Imada et al. 2014). However, details of this relationship between coronal signatures and AR evolution are not clear due to the lack of long-term monitoring with high-enough spatial resolution. Because flares may be triggered by small-scale magnetic structures (e.g. Bamba et al. 2013), the triggering regions should also be inspected with high-resolution spectroscopy. The obtained data will be compared with numerical simulations to identify their MHD instability modes, which could lead to the ability to predict flares in the near future.

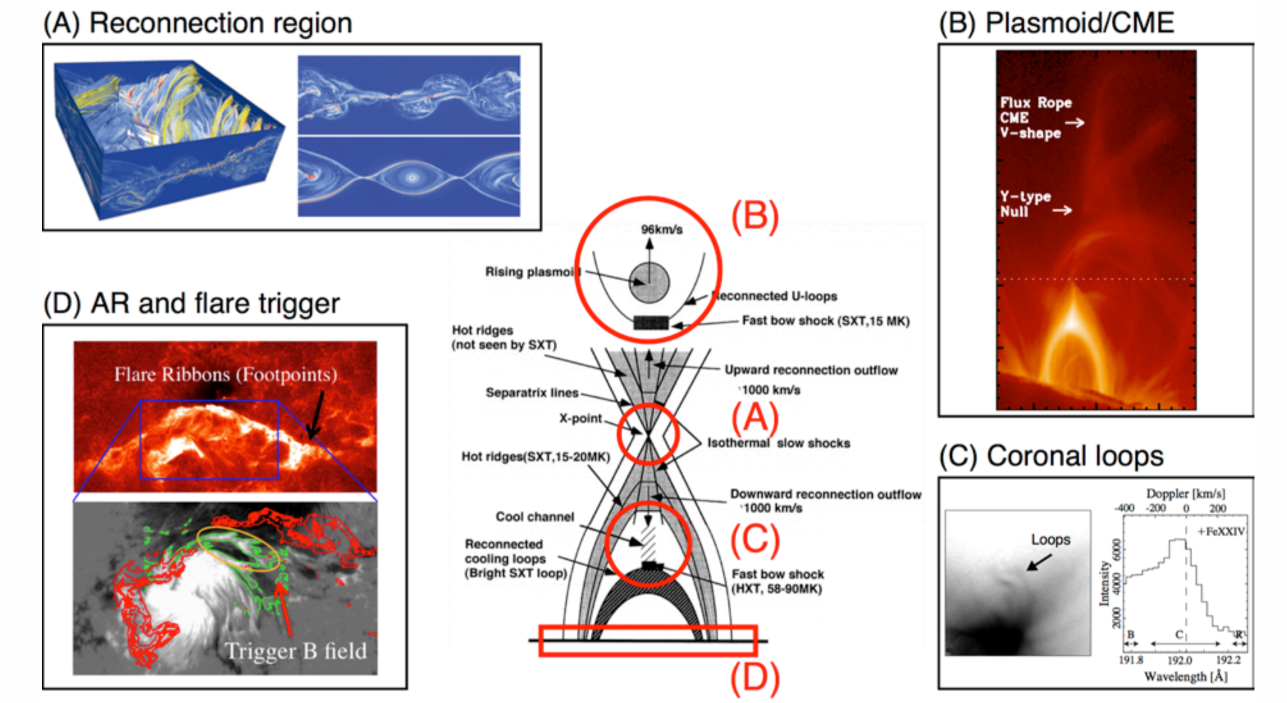

Figure 3.2: Standard flare model (center: Tsuneta 1997) with observations and numerical simulations in each feature. (A) A numerical simulation of the reconnection region (Daughton et al. 2011). (B) Erupting plasmoid and reconnecting current sheet observed by SDO/AIA (Liu et al. 2013). (C) Downward flowing loop signatures above a flare loop (Imada et al. 2013). (D) Flare eruption in an AR with flare-triggering fields (Bamba et al. 2013).

3.2. Goals and objectives: new scientific steps the proposed concept aims to achieve in the science area
提案するミッションコンセプトは当該分野になにをもたらそうとするのか

In order to advance our understanding of the mysterious Sun, especially of the origin of the hot solar atmosphere and the occurrence of the solar flares, the Solar-C_EUVST mission concept tackles the scientific objectives in section 2 by taking the following unique approaches:

A. To seamlessly observe all the temperature regimes of the atmosphere from the chromosphere to the corona simultaneously,

B. To resolve elemental structures of the solar atmosphere and track their changes with sufficient cadence, and,

C. To obtain spectroscopic information on dynamics of elementary processes taking place in the solar atmosphere.

This mission concept provides a completely new set of spectroscopic tools to examine the solar atmosphere. The goals and objectives of this mission, together with a set of specific observing tasks, are described in the rest of this subsection. These shall be the significant steps toward the complete understanding of thermodynamics working in the Sun.

I-1: Nanoflares, tiny magnetic reconnection events, are a possible mechanism for heating the corona if the total amount of energy released by nanoflares is significant. This is the reason why the definitive measurement of the occurrence rate for small-energy heating events is essential. Solar-C_EUVST will evaluate the nanoflare hypothesis by extending the observable energy range down to $\sim 10^{24}$ erg, i.e., about one order better than before (I-1-1 in Table 2.1) thanks to the high spatial resolution (0.4"). The nanoflare heating model predicts transient hot (>5 MK) and fast plasma flows (~100 km/s), that is attempted to be captured by the high-sensitivity spectroscopic observation (I-1-2 in Table 2.1). The high spatial resolution is crucial to clarify where and how nanoflare heating occurs in association with the fine magnetic structures in the corona (I-1-3&4 in Table 2.1).

I-2: The wave heating hypothesis suggests that MHD waves, especially the Alfvén waves, propagate upwards along the magnetic field lines from the solar surface and dump their energy to heat the atmosphere. The spectroscopic capability of Solar-C_EUVST will allow precise measurements of velocity fluctuations caused by transverse oscillation of magnetic fields (I-2-1 in Table 2.1). The seamless coverage of all temperature regimes is essential to catch the propagation of Alfvén waves from the chromosphere to the corona. The high spatial resolution is also critical to observe fine magnetic structures interacting with waves and generating turbulent plasma motions, which is predicted by the theories of thermalization process (I-2-2 in Table 2.1). The plasma diagnostics by Solar-C_EUVST will be complemented by high resolution magnetic field observations from the ground-based telescopes, providing a complete picture of injection, propagation, and dissipation of the waves (I-2-3 in Table 2.1). These observations provide quantitative understanding of how much energy flux is carried by the Alfvén waves and where the energy is dissipated.

I-3: Spicules are the fundamental constituents in the chromosphere and considered to be the key player in channeling the chromosphere and corona by dynamic jets. Solar-C_EUVST will trace thermal evolution of spicules from 2×10^4 K in the chromosphere to higher than 1 MK in the corona by utilizing its seamless coverage over the whole temperature range as well as high spatial resolution enough to discern each spicule. Thermodynamic properties obtained by the spectroscopic observations enable to estimate energy and mass flux into the corona carried by spicules (I-3-1 in Table 2.1). Because spicules originate in the photosphere and lower chromosphere, their driving mechanisms are investigated by joint observations with ground-based telescopes (I-3-2 in Table 2.1).

I-4: The solar wind is the plasma flowing along open field lines into the heliosphere. It is expected to find clear evidence of acceleration by Alfvén waves as it flows away from the corona. The high-sensitivity spectroscopic capability of Solar-C_EUVST aims to get profiles of velocity, temperature, and density along field lines from a faint source region near the surface to the upper corona (I-4-2 in Table 2.1). The measurements yield the height dependence of the Alfvén wave amplitude and its relationship with the plasma flow and temperature for different coronal structures such as polar plumes and inter-plumes (I-4-2 in Table 2.1). It provides a clue to resolve the discrepancy between theory and observation on how much the Alfvén wave dumps their energy to drive the flow.

II-1: Magnetic reconnection is one of the fundamental processes for converting magnetic energy into the thermal and kinetic energy of the plasma. This process occurs much faster than is predicted by classical theory. Solar-C_EUVST will observe the dynamics of magnetic structures to understand the mechanisms that lead to fast magnetic reconnection in partially or fully ionized plasmas. Solar-C_EUVST will test reconnection models (e.g., Sweet-Parker, Petschek, or plasmoid-unstable type reconnection) by observing the velocity, temperature, density, ionization rate in and around the shocks, and magnetic islands of the reconnection region (II-1-1 in Table 2.1). The high spatial and temporal resolution will allow us to study chromospheric evaporation produced by reconnection not only at coronal temperatures but also at low temperatures deep in the transition region and chromosphere (II-1-2 in Table 2.1). This will determine how much energy is released through magnetic reconnection. The observation of magnetic reconnection in the chromosphere by Solar-C_EUVST will clarify the role of the fast reconnection process in weakly ionized plasma (II-1-3 in Table 2.1).

II-2: Understanding of the accumulation and release of free magnetic energy is one of the last pieces of the "solar flare" puzzle. To identify the signatures of global energy buildup, Solar-C_EUVST will perform long-term, wide-field monitoring of the AR corona and investigate the evolution of bulk and turbulent (i.e. non-thermal) plasma velocities (II-2-1 in Table 2.1). By taking advantages of its high spatial, temporal, and spectral resolution, Solar-C_EUVST will focus on the core of the AR and give us detailed information of the flow fields around the flare-triggering site (II-2-2 in Table 2.2). These observables are critically important not only for clarifying the physical conditions and MHD instability modes of the flare eruptions but also for building the algorithms for flare prediction.

Some of the objectives above mentioned require measurements of magnetic fields, although no polarimetric capability is included in the measurements of Solar-C_EUVST. Morphological patterns of the intensity and velocity are only a tracer of the magnetic field structures. A mitigation is, however, to extensively coordinate its observations with ground-based observatories, especially DKIST, which will provide measurements of photospheric and chromospheric magnetic fields with high spatial resolution, although the field of view is limited. These coordinated observations will be essential for evaluating the energy flux carried by waves from the chromosphere toward the corona.

3.3. The compelling nature of the proposed mission concept and its relationship to past, current, and future other investigations and missions.
提案するミッションコンセプトの強みと過去，現在，未来の他のミッション，研究・探査との関係

Before arguing the compelling nature of the proposed mission concept in section 3.3.2, current and future related missions are briefly described in section 3.3.1.

3.3.1 Past, current, and future

<u>Japanese Solar Missions</u>

Three solar physics missions have been launched by ISAS/JAXA in the past 40 years: Astro-A (Hinotori), Solar-A (Yohkoh) and Solar-B (Hinode). Yohkoh and Hinode have been International Partnership Missions with the US (NASA) and the UK (PPARC, STFC), and Europe (ESA on Hinode). All three missions have been highly successful and are providing a wealth of discoveries. Based on these successes, we have established reliable and strong partnerships with the US and Europe. Solar-C_EUVST will build upon this rich tradition.

Launched in 1981, Hinotori provided the first hard X-ray images of solar flares. It clarified the importance of hard X-ray imaging observations for understanding particle acceleration in the flares. Yohkoh, launched in 1991, was devoted to observations of solar flares and the solar corona using a combination of soft and hard X-ray imaging, and non-imaging spectroscopy. It is not an exaggeration to say that the bulk of our knowledge of high-energy solar phenomena has come from Yohkoh. For example, Yohkoh provided strong observational support for concluding that magnetic reconnection plays a key role in the energy release process for flares.

Hinode, launched in 2006, observes photospheric vector magnetic fields, and their energetic and dynamical consequences in the corona. Hinode carries three main instrument packages: a Solar

Optical Telescope (SOT), an X-Ray Telescope (XRT), and an Extreme-Ultraviolet Imaging Spectrometer (EIS). The SOT has provided photospheric/chromospheric images and the spectro-polarimetric data for measurements of the vector magnetic field in the photosphere, having 0.2"-0.3" spatial resolution. The vector magnetograms produced by Hinode have the highest sensitivity and spatial resolution ever obtained. The EIS has discovered extensive outflows at the edges of active regions that could be important contributors to the solar wind and is providing valuable information on solar flares, coronal heating, and mass inputs from the chromosphere. The XRT has provided new insights into hot plasma created by the dynamical events in solar flares and ARs.

Related Solar Missions Currently Running

SoHO : Solar and Heliospheric Observatory, launched in 1995, is an international project between ESA and NASA to study the Sun from the interior to the outer corona, including the solar wind. CDS (Coronal Diagnostic Spectrometer) and SUMER (Solar Ultraviolet Measurements of Emitted Radiation) detected EUV and VUV emission lines in the chromosphere through the transition region to the corona, providing diagnostic information on the solar atmosphere (flows, temperature, and density). Currently, only some of the instruments on SoHO are still providing data for monitoring the full Sun, and none of them has any overlap with the high-resolution instruments.

RHESSI : Reuven Ramaty High Energy Solar Spectroscopic Imager is a NASA SMEX mission launched in 2002. RHESSI's primary mission is to explore the basic physics of particle acceleration and explosive energy release in solar flares. This is achieved through imaging spectroscopy in X-rays and gamma-rays to reveal the locations and spectra of the accelerated electrons and ions and of the hottest flare plasma. Its limited spatial resolution does not allow it to address the issue of magnetic reconnection, which Solar-C_EUVST will challenge.

SDO : The Solar Dynamics Observatory, launched in 2010, carries three instruments. HMI (Helioseismic and Magnetic Imager) and AIA (Atmospheric Imaging Assembly) are instruments for full-Sun observations. HMI is designed for measuring the magnetic field on the surface. AIA images the chromosphere and the corona in multiple UV wavelengths to link changes in the outer atmosphere to the surface. EVE (Extreme Ultraviolet Variability Experiment) measures the solar EUV irradiance (i.e. no spatial resolution) with high spectral resolution, temporal cadence, and precision. Although SDO does not provide any spatially resolved spectroscopic information, it will supply context coronal images and surface magnetograms that have a high potential for synergy with the high-resolution EUVST data.

IRIS : Interface Region Imaging Spectrograph is a NASA SMEX mission launched in 2013. IRIS obtains UV spectra with high resolution in space (0.33-0.4") and time (4-8 s) focusing on the chromosphere and lower transition region. IRIS has very little coverage of lines formed in the hot transition region or corona, and thus cannot provide the observation that seamlessly cover the whole temperature range of the outer solar atmosphere.

Heliospheric Missions in the Near Future

PSP : Parker Solar Probe (to be launched in summer 2018) is a mission to trace the flow of energy through the inner heliosphere and to explore what accelerates the solar wind as well as energetic particles by flying to within 9 solar radii from the solar surface (first close approach in 2024). PSP will carry a suite of four instruments (three in-situ measuring instruments and one remote-sensing instrument) designed to study magnetic fields, plasma and energetic particles. WISPR (Wide-field Imager for Solar Probe) will image the solar wind structures as they pass the spacecraft. PSP will probe the microphysics of the outer corona and solar wind in a unique manner, but will not observe atmospheric conditions near the solar surface. Solar-C_EUVST is therefore a complement to PSP.

SO : Solar Orbiter (to be launched in 2020) will provide the first-ever images of the Sun from an out-of-ecliptic viewpoint (up to 25° of solar latitude during the nominal mission phase until 2027, and up to 34° during the extended phase) by in-situ and remote-sensing instruments. Among the 6 remote-sensing instruments, SPICE (Spectral Imaging of the Coronal Environment) will obtain UV/EUV spectra with 4" spatial resolution (equivalent to 1.3" at 1 AU at the closest approach of 0.3 AU) to detect plasma properties of the Sun's on-disc corona. STIX (Spectrometer/Telescope for Imaging X-rays) provides imaging spectroscopy of X-ray emission to measure timing, location, and spectra of accelerated electrons as well as high temperature plasmas associated with flares and microflares. Although SO does not measure imaging spectroscopic data with high spatial and temporal resolution, it will give us observations from different view angles, which has a very high potential for synergy by coordinating with Solar-C_EUVST (e.g., 3D tomography analysis).

Missions Under Study

MUSE : Multi-Slit Solar Explorer is a proposed NASA Small Explores (SMEX) mission currently under phase A study for investigating the dynamics of the corona using novel spectral imaging techniques. MUSE will obtain EUV spectra and images with the highest spatial (0.3") and temporal (1-4 s) resolution in a large FOV, enhanced by multi-slit spectroscopy of a few selected spectrum lines. Although MUSE has limited temperature coverage as well as diagnostic capability (e.g., temperature, density diagnostics), MUSE is a revolutionary type of coronal imager. It is really T-07 in the NGSPM-SOT report and is very complementary to Solar-C_EUVST or T-09, not redundant to or directly competitive with it.

FOXSI : The Focusing Optics X-ray Solar Imager is a proposed NASA SMEX mission currently under phase A study for investigating acceleration of energetic particles and the heating of the solar corona to high temperatures. The FOXSI SMEX concept is based on the FOXSI sounding rocket payload, which was flown in 2012 and 2014. A third launch is planned for 2018. FOXSI's direct imaging will provide a much higher dynamic range than previous imagers, such as RHESSI. FOXSI would complement Solar-C_EUVST by observations of higher temperature plasma than is accessible with EUV spectroscopy. FOXSI, however, would have significantly lower spatial resolution (8") than Solar-C_EUVST and not provide information such as Doppler shifts and plasma densities.

3.3.2 The compelling nature of the proposed mission concept

The Solar-C_EUVST mission will generate spectroscopic observations with vastly improved spatial, temporal, and temperature resolution. These improved capabilities will allow for two types of observations that have previously been impossible. First, the high spatial resolution of Solar-C_EUVST will allow for very small scale structures to be observed over the full range of temperatures in the solar atmosphere (see Figure 3.3). This will allow the plasma properties of these structures to be observed directly for the first time. Such spectroscopic observations will provide diagnostics of Doppler shifts, non-thermal velocities, temperature, and density at a spatial resolution and cadence currently only achievable by imaging instruments. This ability to observe 2D plasma properties at high cadence for the complete atmosphere has the potential to be as transformational as the first high-resolution imagers of the corona. Detailed comparisons of the performance of Solar-C_EUVST and other spectroscopic missions will be presented in section 6.2.5.

1) Spatial resolution

Observations made with Hinode and other missions indicate that the spatial resolution required for observations of elemental structures and processes is within our reach. This conclusion is based in part on the Hinode/SOT observations that show that the typical chromospheric structures (such as spicules, Pereira et al. 2012) are 300 km (0.4"). Consistent with this, studies of coronal rain, condensations of million-degree plasma that form in the corona when hot loops cool very suddenly, show widths of about 300 km (Antolin & Rouppe van der Voort 2012). Similarly, estimates of the filling factor of EUV coronal loops derived by comparing the density and observed intensity suggest loop widths of several hundred km (Hinode/EIS observation by Warren et al. 2008). Finally, the modeling of evolving loops at 1 MK temperatures also suggests that they could be composed of only a few strands, each several hundred km in width (Brooks et al. 2012). The Solar-C_EUVST mission will attempt to resolve such elemental structures. It is important to note that there is almost certainly a distribution of loop widths in the solar atmosphere, one that may extend down to loops only a few tens of km wide. The accumulated evidence, however, suggests that there is a strong peak in this distribution near several hundred km (e.g., Aschwanden & Peter 2017).

2) Temporal resolution

We need measurements of both the fast time-scale MHD perturbations of structures due to waves, as well as measurements of the slowly varying magnetic structures subject to quasi-static deformation. Such measurements will allow us to determine the relationship between the field topology and atmospheric heating, as well as the energy flux carried by waves and their dissipation. As another example of the necessity of high time cadence, let us consider observations of extremely high temperature emission (>5 MK). High temperature plasma is produced immediately after an impulsive energy input (during a flare, CME, jet, or nanoflare). Because the lifetime of such high temperature emission can be very short (~ a few seconds), high temporal resolution observations are critical. In order to achieve the required high temporal resolution, the effective area for Solar-C_EUVST is ~ 10 times larger than previous instrumentations (see Figure 6.1).

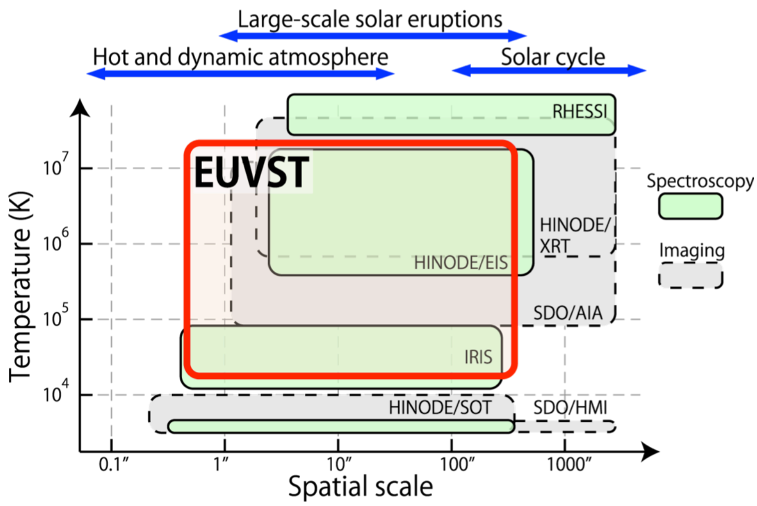

Figure 3.3: Characteristics of Solar-C_EVUST in terms of the temperature and spatial coverage, as compared with the currently running missions.

3) Temperature coverage

Another unique approach of the Solar-C_EUVST mission is to perform photometric and Doppler observations without temperature gaps from the chromosphere to the corona. Hinode is blind to much of the transition region and has no diagnostic capability in the chromosphere. It has become clear from analyses of Hinode data that these observational gaps prevent complete understanding not only of these layers, but also part of the corona and heliosphere, since the solar atmosphere is a coupled system. Solar-C_EUVST will rectify this with an instrument that simultaneously observes emission from the chromosphere, transition region, and corona at similar high spatial resolution (see Figure 3.3). This is one of the most innovative and challenging properties of this instrument.

4. Launch constraints

4.1. Target launch date and rough schedule [18-1-1. 18-2-1]
めざす打ち上げ時期と大まかなスケジュール

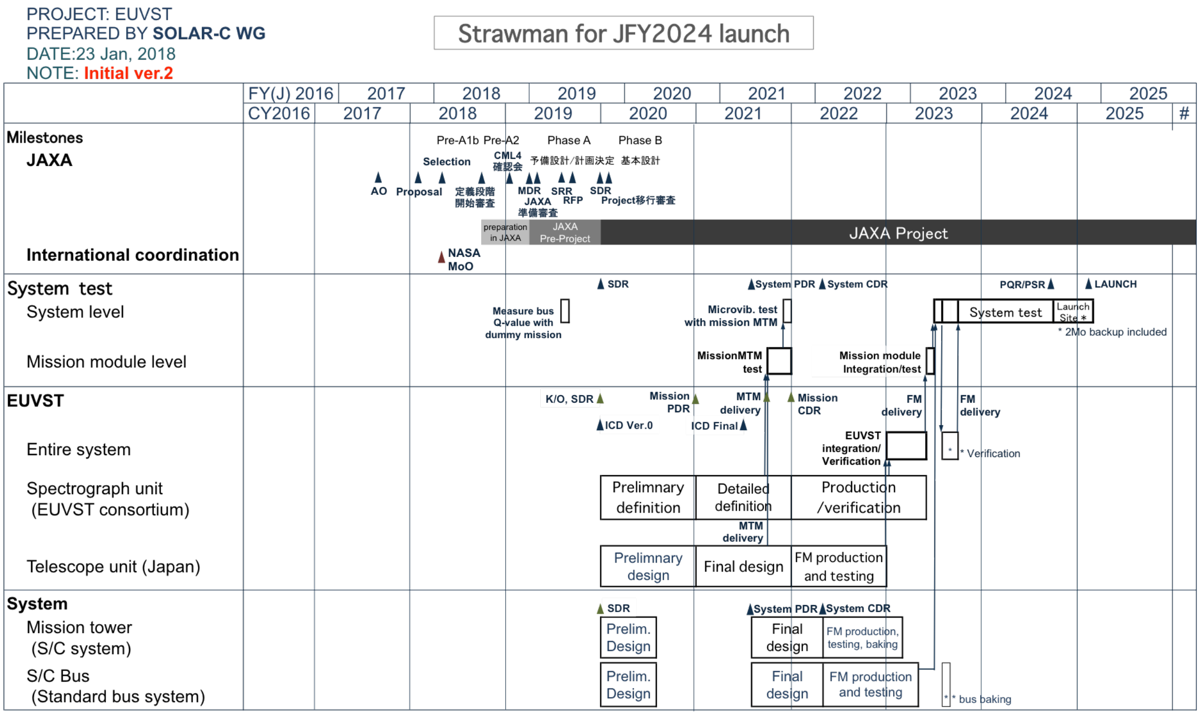

Figure 4.1: Strawman schedule

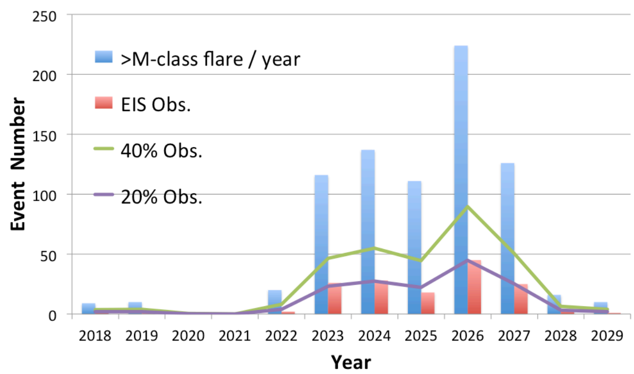

Figure 4.2: Predicted number of large (>M-class) flares in each year. Red columns give the number of large flares actually observed by a similar spectrometer EIS. The solar minimum is assumed in 2019, with shifting Hinode's statistics from 2006 to 2017.

Figure 4.1 is the overall strawman schedule for the launch on February 2025 (Japanese Fiscal Year (JFY) 2024). This is the earliest schedule. For maximizing the scientific return by increasing the possibility of capturing many large flares and by coordinating with observations by SO (expected to be over 25° helio-latitude around 2024) and the PSP (expected to have a close approach <10 solar radius around 2025), the launch in JFY 2024 is preferable. JFY2026 is also acceptable, based on the predicted number of flares (Figure 4.2). In the strawman schedule (Figure 4.1), the time scale before System Definition Review (SDR) is very tight for starting the project from the beginning of 2020.

4.2. Constraints from the launch vehicle (launch performance, envelope etc.) [13-2-1] 打ち上げ手段からの制約（打ち上げ能力，搭載エンベロープなど）

An Epsilon vehicle after H3 synergy update (completed by 2021) is assumed. The launch performance is the same as the performance of the 2nd flight (December 2016 for ERG), the details of which are described in Epsilon Rocket Users' Manual (NC, March 2016).

Table 4.1: Accuracy (3σ) of the orbit installation. ( ) : Orbit parameter

Configurations / Orbits		Perigee altitude [km]	Apogee altitude [km]	Inclination [deg]
Without PBS	LEO	±25 (250)	±100 (500)	±2.0 (31.0)
	Elliptical orbit	±25 (250)	±2000 (30700)	±2.0 (31.0)
With PBS	LEO	±20 (500)	±20 (500)	±0.1 (30.5)
	SSO	±20 (500)	±20 (500)	±0.2 (97.4)

For installation to a sun synchronous polar orbit (SSO), PBS (Post Boost Stage) is required to guarantee the accuracy of the installed orbit. The accuracy is listed in Table 4.1; for the SSO, +/-20 km in the altitude and +/- 0.2 degrees in inclination. The maximum weight for the SSO is given in Figure 4.3(a). The Epsilon team (R. Yamashiro) suggests the case that the PBS has a propellent mass of 160 kg; namely, the maximum weight is 590 kg for the height of 600-650 km and 560 kg for 700 km. If more weight is needed for the payload, low earth orbit (LEO) shall be considered. Figure 4.3(b) shows the envelope of the Epsilon rocket nose fairing, in which the proposed mission should be accommodated.

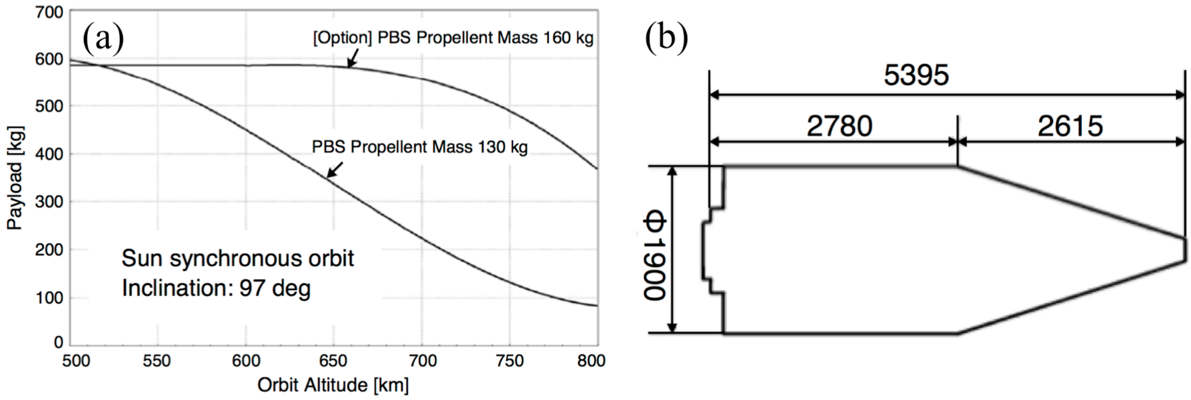

Figure 4.3: (a) The payload weight for a sun synchronous polar orbit. (b) The nose fairing envelope.

5. Scientific investigations of the mission [3-2–1]
ミッションが実施する研究・探査

5.1. Rationale for the investigations [3-2-2][1-3-1]
ミッションが実施する研究・探査の根拠

To achieve the science objectives of the mission which are shown in section 2 (Table 2.1), there are several possible instruments that can be considered. To discuss the rationale for the investigations, we assume a slit-scanning type imaging spectrometer to clarify the points. Note that this type of spectrometer will be chosen by a trade off study described in section 6.2. In this section, Table 2.1 is referred for the number given in science sub-objectives/observing tasks, such as I-1/I-1-1, respectively.

I-1: Quantify the Contribution of Nanoflares to Coronal Heating (Table 5.1)

One of the main science objectives of Solar_C-EUVST will be to quantify the contribution of nanoflares to coronal heating. Since the Skylab era (e.g., Rosner et al. 1978) it has been known that the coronal loops in the core of an AR have temperatures of 3-4 MK. These bright, hot AR loops will be the primary target for this science objective. As is illustrated in Figure 5.1(a), these AR core loops can be observed in emission lines from Fe XVIII. This figure, which shows an observation with the AIA 94 Å channel, illustrates an imaging observation of the Fe XVIII 93.94 Å line. Solar-C_EUVST will observe the longer wavelength Fe XVIII 974.86 Å line, which has the highest photon flux per unit emission measure of any Fe XVIII transition. The object is to search for faint high temperature emission predicted by nanoflares in all the AR loops.

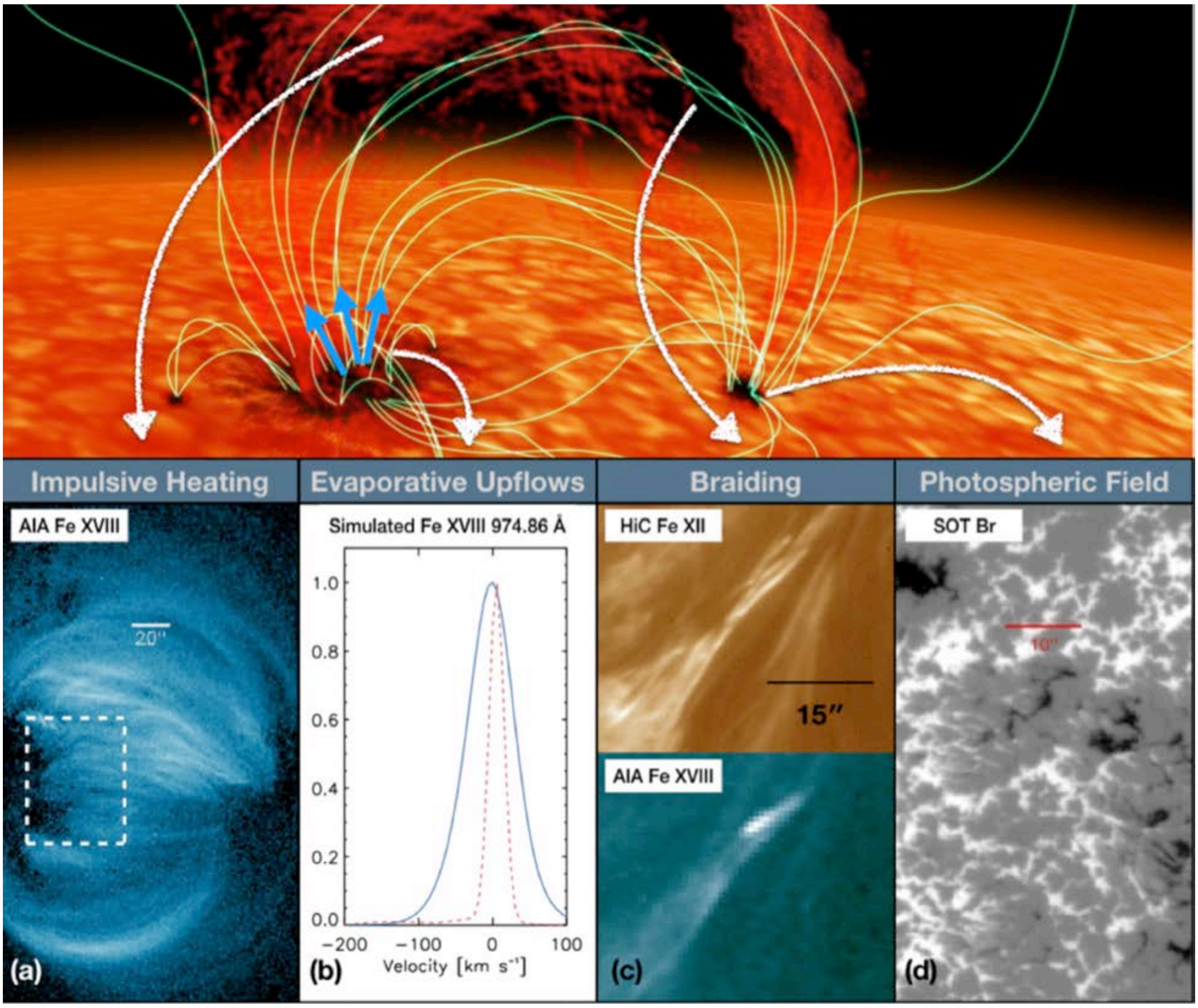

Figure 5.1: (a) SDO/AIA routinely observes transient heating events in Fe XVIII. Solar-C_EUVST will observe them with much higher spatial resolution and cadence and also provide plasma diagnostics such as temperature, density, Doppler shift, and non-thermal broadening, the quantities that should be compared with theories. (b) Solar-C_EUVST will be able to observe the evaporative upflows associated with small-scale heating events predicted by nanoflare models. Here a simulated footpoint profile (blue) and loop-averaged profile (red) are shown. (c) High spatial resolution images from Hi-C show braided loops in Fe XII. These loops are associated with the formation of high temperature plasma. With its high spatial resolution Solar-C_EUVST will observe such events over a very wide range of temperatures. (d) Hinode/SOT observations of the magnetic field at the footpoints of the Fe XVIII loops in panel (a). Similar coordinated observations with high resolution ground-based observatories such as DKIST will allow us to reveal the photospheric changes that drive nanoflares to be identified. Schematic illustration of nanoflare on the top of figure is made by ISAS/JAXA.

The improved spatial resolution and sensitivity of Solar-C_EUVST will allow events with smaller energies to be studied. The most compelling evidence for this comes from the Hi-C sounding rocket experiment, 5 minutes observations of the footpoints of high temperature loops. Hi-C took very high spatial resolution (0.3-0.4") images at a cadence of about 5.5 s. Testa et al. (2013) showed that with the increased spatial resolution and cadence of Hi-C, rapid variations in footpoint intensity could be detected. The estimated energies are ~10^{24} erg for these events. Furthermore, these events could not be detected at the lower spatial resolution and cadence of SDO/AIA.

The first observing task (I-1-1) will be to quantitatively measure the energy of heating events with energies in the nanoflare range (~10^{24}-10^{27} erg) envisioned by Parker (1972). These events can only be detected at the higher spatial resolution (0.3—0.4") and cadence (5.5 s). Solar_C-EUVST will be able to follow nanoflare's evolution in the core of the AR from high temperatures to low temperatures (wide temperature coverage) with high temporal resolution. The spectroscopic observations will also provide electron densities, further improving the estimate of event energies.

These detected events will be used to form a statistical distribution of event energies, which will be compared against the energy requirements of the active corona (see Shimizu 1995 for the seminal paper on this type of analysis).

The nanoflare concept predicts that heating events should be associated with chromospheric evaporation similar to that observed in large flares. As with large flares, the complicating factor is the superposition of emission along the line of sight. As modeled by Patsourakos & Klimchuk (2006), spectral line profiles that have enhancements in the blue wing are expected from nanoflare heating, not completely shifted line profiles. This is illustrated in Figure 5.1(b), which shows that the extent of this enhancement is determined by the amount of energy released and the spatial scale of the energy release. The second observing task (I-1-2) will be to observe these evaporative upflows and compare the observations to model predictions. This will be achieved using sit-and-stare observations of Fe XVIII at a cadence of 5 s or better.

The third observing task (I-1-3) will be to search for the field line braiding envisioned in the Parker model. As is illustrated in Figure 5.1(c), in the Hi-C observations these twisting field lines were associated with the formation of high temperature plasma (Cirtain et al. 2013). Solar-C_EUVST will observe this process over a much wider range of temperatures and also provide the full range of plasma diagnostics that is needed for comparing with theory. This goal will be achieved using the combination of slow (a few minutes) and full spatial resolution (0.4") scans and fast (~ a few 10 s) middle resolution (0.8") scans in a wide selection of spectral lines over a small field of view.

The fourth observing task (I-1-4) requires the same observational parameters as (I-1-3). The important requirement is coordinated observations of the photosphere (Figure 5.1(d)) and low chromosphere by a ground-based telescope.

Table 5.1: Summary of requirements for science objective I-1

<table>
<tr><th rowspan="2">Item</th><th colspan="4">Requirement</th><th rowspan="2">Rationale</th></tr>
<tr><th>I-1-1</th><th>I-1-2</th><th>I-1-3</th><th>I-1-4</th></tr>
<tr><td>Temperature coverage (MK)</td><td colspan="4">0.8-10
(5-10 for nanofare signatures)</td><td>To observe nanoflare heating-cooling cycles. Nanoflare signatures are detected with high temperature lines.</td></tr>
<tr><td>Spatial resolution (arcsec)</td><td>0.4</td><td>0.8</td><td colspan="2">0.4
[high cadence: 0.8]</td><td>0.4" for resolving nanoflare events and subarcsec braiding structures and 0.8" for resolving fine structures at footpoints of coronal loops.</td></tr>
<tr><td>Temporal resolution (s/step)</td><td>5
/0.4"</td><td>1.5
/0.8"</td><td colspan="2">5/ 0.4"
[high cadence: 1.5/0.8"]</td><td>I-1-1: Similar cadence as Hi-C observation (5.5 s).
I-1-2, I-1-3: The exposure time is shorter than the spatial scale (0.8" ~ 600 km) / sound speed 300 km/s, ~2 s.</td></tr>
<tr><td>FOV
($arcsec^2$)</td><td>0.4
×
100</td><td>0.8
×
280</td><td colspan="2">20×100
[high cadence: 20×100]</td><td>I-1-1: The slit on the core of an active region.
I-1-2: Capture both of the footpoints of AR loops.
I-1-3: Capture the entire or a part of coronal loops.</td></tr>
<tr><td>Velocity resolution (km/s)</td><td colspan="4">$V_d \sim 2$
$V_{nt} \sim 5$</td><td>Enough to resolve plasma flows (Doppler and turbulent components) caused by tiny energy releases.</td></tr>
<tr><td>Observation duration & total days</td><td colspan="4">~1 hour
15 days each</td><td>Longer than the evaporation-condensation cycle.
Repeated measurements for statistical studies</td></tr>
<tr><td>Co-alignment</td><td colspan="3">n/a</td><td>√</td><td>For precise co-alignment with ground-based data. Simultaneous slit jaw imaging to know where the slit is located on solar images.</td></tr>
</table>

1": 730 km, V_d: Doppler velocity, V_{nt}: nonthermal velocity (e.g., turbulence)

I-2. Quantify the Contribution of Wave Dissipation to Coronal Heating (Table 5.2)

The magnetized solar atmosphere is filled with a rich assortment of waves that are an important source of energy flux. The exact amount of energy flux they transport and the fraction of the energy dissipated into various structures still need to be determined. In particular, Alfvén waves have long been proposed as a candidate mechanism to transport magneto-convective energy from the convection zone into the solar atmosphere where they can heat plasma to coronal temperatures and accelerate solar wind through dissipation of their non-thermal energy (e.g. Suzuki et al. 2005, van Ballegooijen et al. 2011). Because Alfvén waves are subject to wave reflection (van Ballegooijen et al. 2011), as the Alfvén speed increases from about 10 km/s in the chromosphere to more than 1000 km/s in the corona, especially in the transition region, only a fraction of the wave energy can be transmitted into the corona. It is thus critically important to clarify how the velocity fluctuation propagates from the chromosphere to the corona through the transition region. This is the first observing task (I-2-1) of the science objective that is attempted by simultaneous observations of emission lines from 0.02 to 3 MK in the atmospheres. If Alfvén waves carry a significant amount of the energy transmitted in the corona, 10^5 erg/cm^2/s, a velocity amplitude of Alfvénic waves is expected to be of the order of 10 km/s in the corona. Recent imaging observations have detected signatures of transverse oscillations in chromospheric structures (Figure 5.2(a)), suggesting the potential of waves in powering the solar atmosphere (De Pontieu et al. 2007a; Okamoto et al. 2007; Jess et al. 2009; Okamoto & De Pontieu 2011). Alfvénic waves have been observed in the corona by a coronagraph observation (e.g. Tomczyk et al. 2007), but the velocity amplitude is smaller than 1 km/s, giving an estimate of flux which is much smaller than is required for coronal heating. This may be largely underestimated due to the integration of signals over unresolved features in the coronagraph observation. Thus, spatially resolving coronal structures with Solar-C_EUVST is essential to accurately determine the velocity amplitude of waves and to evaluate the magnitude of their energy flux.

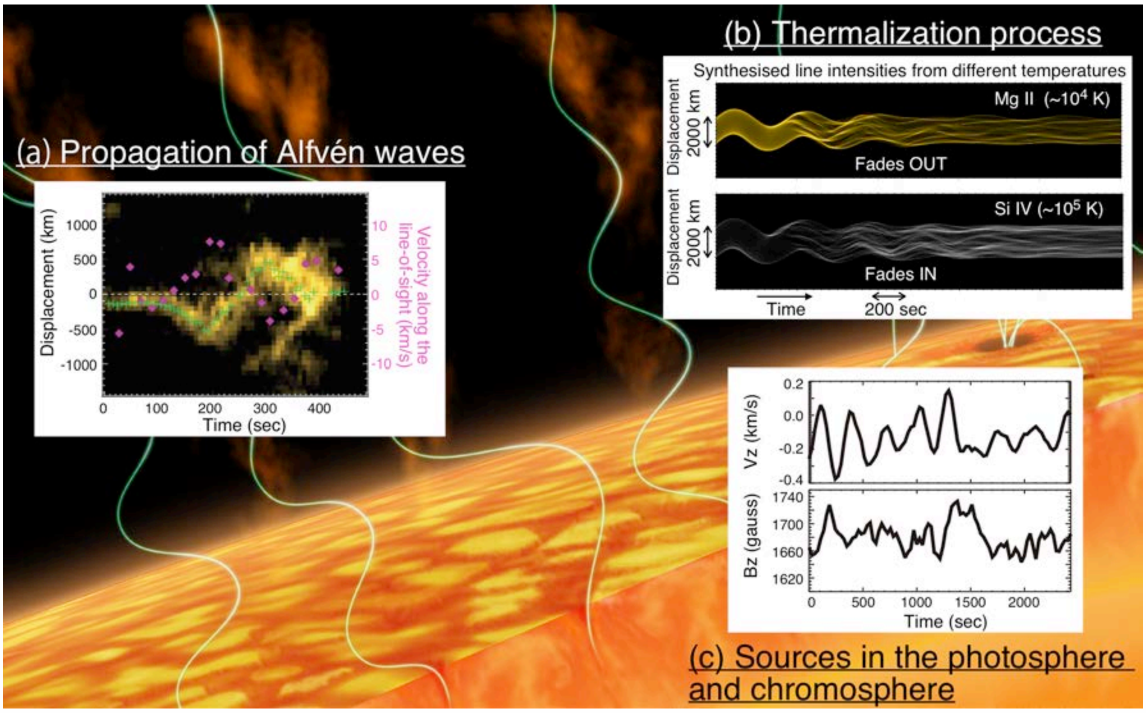

Figure 5.2: (a) Observation of a prominence thread structure indicating lateral and line-of-sight oscillation (Okamoto et al. 2015), (b) synthesized line intensities from the chromosphere (10^4 K) and transition region (10^5 K) indicating appearance in the hotter line as a result of thermalization of the Alfvén wave (Antolin et al. 2015), and (c) observation of velocity and magnetic fluctuation to explore a source of the Alfvén wave (Kanoh et al. 2016).

The theory for the wave that Alfvénic waves interact with density structures in the transition region and corona, which causes nonlinear evolution of the velocity amplitude causing mode conversion and turbulence, leading to dissipation and heating (e.g. Okamoto et al. 2015, Antolin et al. 2015, Matsumoto 2016) (Figure 5.2(b)). In the second task (I-2-2), Solar-C_EUVST will measure spectroscopically how amplitudes and phases of velocity fluctuation vary and are correlated among emission lines from the chromosphere to the corona. The observation is done along with observations of the density structure with the sub-arcsec resolution, needed to characterize the transverse variation of the atmosphere structure. Solar-C_EUVST should scan a footpoint region of a magnetic field line to achieve a temporal cadence shorter than 1 min with the FOV narrower than 10" to get high spatial and velocity resolution to yield key information on the wave propagation and dissipation processes. Another observing mode is to map a 200 Mm wide region in a time shorter than the Alfvén speed (~1000 km/s in corona), i.e., less than 200 s in order to follow the wave as it moves through the corona and see its influence on the upper corona. This will be achieved by repeated raster scannings with a wide slit (1.6"). Because Solar-C_EUVST is sensitive only to atmospheric layers hotter than 0.02 MK, sources of the Alfvén waves in the photosphere and chromosphere are studied by coordination with ground-based telescopes, such as DKIST.

Table 5.2: Summary of requirements for science objective I-2

Item	Requirement			Rationale
	I-2-1	I-2-2	I-1-3	
Temperature coverage (MK)	0.02-3			To observe velocity fluctuation which propagate from the chromosphere to the corona through the transition region.
Spatial resolution (arcsec)	0.4 [high cadence: 1.6]			For resolving thread-like structures through the chromosphere to the corona, 0.4" is required. For achieving high S/N and high temporal resolution, 1.6" is acceptable.
Temporal resolution (s/step)	2/0.4" [high cadence: 0.5/1.6"]			We make use of a fast scan to trace the propagation of Alfvén waves whose speed is 1000 km/s in the corona.
FOV (arcsec^2)	10×100 [high cadence: 280×280]			It is possible to cover the wavelength of Alfvén waves with a period shorter than 200 sec. 1000 km/s × 200 s ~ 200 Mm, corresponding to 280".
Velocity resolution (km/s)	$V_d \sim 2$			For measuring transverse oscillations 10 km/s responsible for energy transfer.
Observation duration & total days	~1 hour 15 days each			Cover more than 10 wave periods where the typical period is 3 to 5 minutes. Repeated measurements for statistical studies
Co-alignment	n/a		√	For precise co-alignment with ground-based data. Simultaneous slit jaw imaging to know where the slit is located on solar images.

1": 730 km, V_d: Doppler velocity

I-3. Understand the formation mechanism of spicules and quantify their contribution to coronal heating (Table 5.3)

Observations of spectral lines from the chromosphere, such as Ca II, have clearly revealed that the chromosphere is dominated by a multitude of thin (300 km, i.e., 0.4" width, see Figure 5.3), dynamical, jet-like extrusions called spicules. They have a typical upflow speed of 50 to 200 km/s and a lifetime of 20 s to 300 s (e.g. Pereira et al. 2012). The origin of spicules is still not understood and the contribution of spicules to the million degree corona has not been determined. Spicules have been reported to produce broadening and asymmetries in coronal spectral line profiles observed by Hinode/EIS, whose spatial and temporal resolution is 2" and 300 s, respectively (De Pontieu et al. 2009). Such observations have led to the hypothesis that spicules are an important contributor of mass and energy to the corona, although the sizes and temporal evolution of spicules are well below the resolution of current UV and EUV spectrometers such as Hinode/EIS. Spatial and temporal resolution in the spectroscopic measurements is crucial to understand whether spicules provide a significant contribution to heating at transition region or coronal temperatures. IRIS achieved sufficient spatial resolution to resolve spicules (Pereira et al. 2014), but it provides temperature coverage only in the chromosphere and the low transition region. Although radiative MHD simulations have some success in reproducing spicules, their role in coronal heating (Figure 5.3) is still not clear. Solar-C_EUVST will allow us, for the first time, to trace individual spicules seamlessly as they rise into the corona by monitoring the evolution of the line profiles formed at increasingly higher temperatures. In the first task (I-3-1), repetitive scans for a 10" wide area are needed with high spatial resolution (0.4") as well as high cadence (180 s < life time of spicules). Although Solar-C_EUVST cannot observe the photosphere and low chromosphere, the second task (I-3-2) will be achieved through coordination with ground-based telescopes such as DKIST.

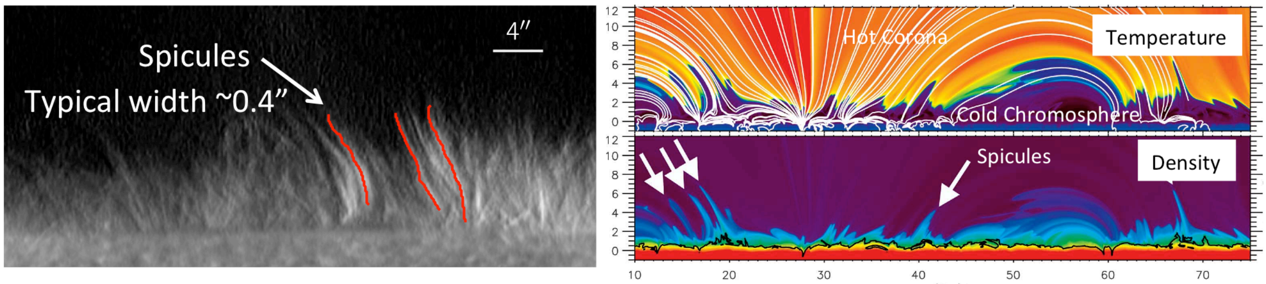

Figure 5.3: Left) Sample spicule Ca II H image observed by Hinode/SOT (Pereira et al. 2012). The typical spicule width can be estimated to ~0.4". Right) Spicule-like features in a radiative MHD simulation (Martínez-Sykora et al. 2017). We can clearly see that the cold spicules penetrate into the hot corona.

Table 5.3: Summary of requirements for science objective I-3

Item	Requirement		Rationale
	I-3-1	I-3-2	
Temperature coverage (MK)	0.02-3		For observing the chromosphere, transition region, and corona simultaneously.
Spatial resolution (arcsec)	0.4		For resolving sub-arcsec spicule structures in the chromosphere and their counterparts in transition region and corona.
Temporal resolution (s/step)	2/0.4"		For scanning a 10" wide area within 1 min. Shorter than the life time of spicules (20~300 s).
FOV (arcsec^2)	10×100		The entire structure of spicules and chromospheric jets should be observed.
Velocity resolution (km/s)	$V_d \sim 2$		Enough to resolve upward speed of spicules.
Observation duration & total days	~1 hour 15 days each		Longer than the typical transient phenomena in chromosphere (e.g., jets). Repeated measurements for statistical studies
Co-alignment	n/a	√	For precise co-alignment with ground-based data. Simultaneous slit jaw imaging to know where the slit is located on solar images.

1": 730 km, V_d: Doppler velocity

I-4. Understand the Source Regions and the Acceleration Mechanism of the Solar Wind (Table 5.4)

The source regions of the fast and slow solar wind are still under debate. Regarding the fast solar wind sources, polar plumes (structures are about 10" wide at the base of the corona that have been tracked while they expand super-radially up to about 10 solar radii and beyond, and their lifetimes are about 10 hour, Wilhelm et al. 2011) and inter-plume regions, which extend from coronal holes into the high corona and probably link to the solar wind, have been proposed as sources. Since smaller outflow speeds are detected at the base of polar plumes (0.7~0.9 MK), inter-plumes (1~1.3 MK) have been considered to be the fast wind source. However, contradictory results have been obtained from off-limb observations, with inter-plume regions showing larger outflow velocities in some studies (e.g., Teriaca et al. 2003) and plumes themselves exhibiting higher outflow velocities in others (Gabriel et al. 2003). For the slow solar wind, Hinode/XRT and Hinode/EIS have revealed the presence of persistent flows (V ~ a few 10 km/s, T ~ a few MK) at the edges of ARs (e.g., Sakao et al. 2007) (size of AR ~ 280×280 arcsec^2), which show the same compositional signature as the slow wind observed at Earth (Brooks & Warren 2011). On the other hand, streamers in the higher corona have also been proposed as one of the slow solar wind sources as a result of far off-limb observations (e.g., Raymond et al. 1997). So far, compelling observational evidence that definitively identifies the source regions of the solar wind is still controversial, but it could be that a combination of lower atmospheric sources (such as AR outflows) and higher altitude sources (such as streamers) together provide the total mass flux of the slow wind (Brooks et al. 2015, Figure 5.4a).

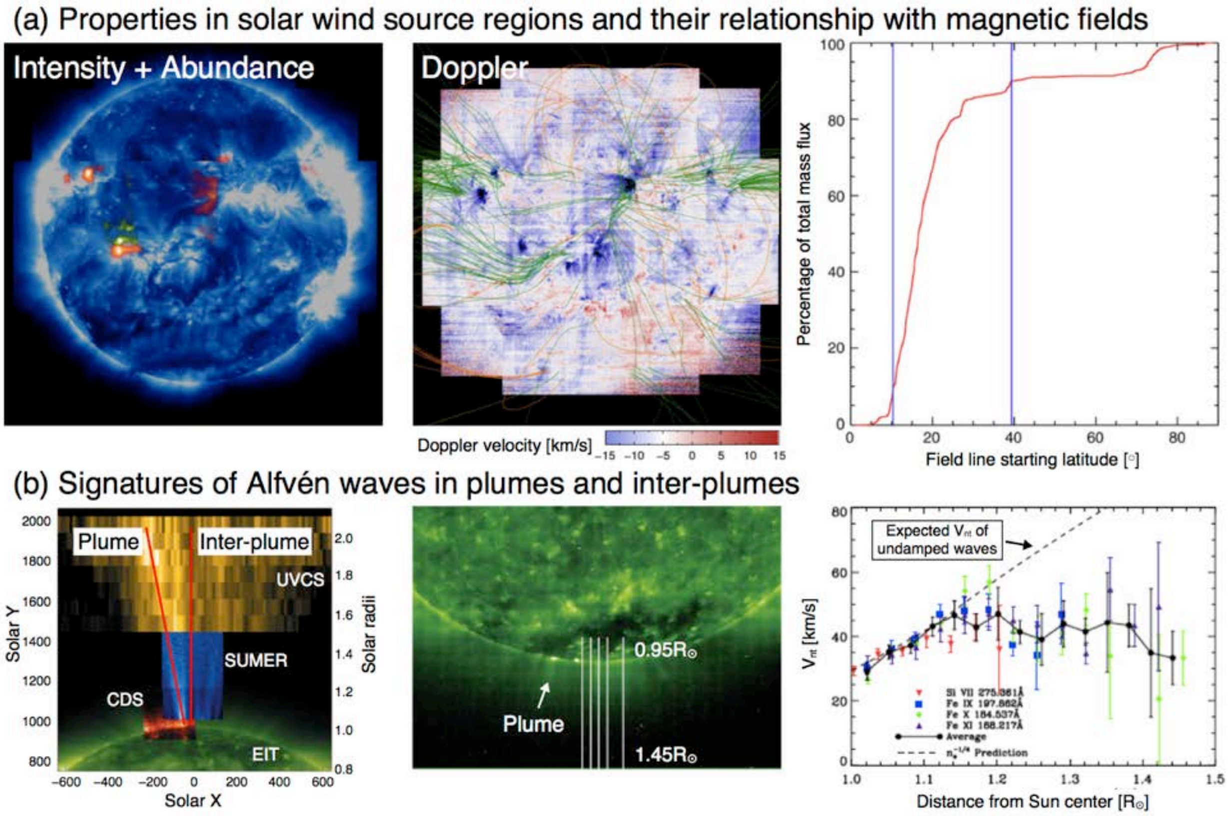

Figure 5.4: (a) Left) Plasma properties in solar wind source regions and their relationship with magnetic fields (Brooks et al. 2015). Left) full-Sun AIA 193Å composite intensity image (blue) with solar wind source regions (red and green), which is identified by abundance. Center) Overlay of magnetic field lines from the potential field extrapolation calculation on the Fe XIII 202.044 Å Doppler velocity map from Hinode/EIS. Right) Percentage of total mass flux as a function of magnetic field line-starting latitude (red). The vertical blue lines on the left and right side mark the latitude of 11° and 40°. (b) Signatures of Alfvén waves in plumes and inter-plumes. Left) Plume and inter-plume observed by multiple telescopes (Teriaca et al. 2003). Center) Slit positions of Hinode/EIS for the observation of the right panel overlaid on the SoHO/EIT 195 Å image. Right) off-limb observation of the non-thermal velocity (V_{nt}) from the strongest observed lines (symbols). The dashed line gives the predicted trend, proportional to the electron density n as $n^{-1/4}$, for undamped waves. The observed behavior of V_{nt} may be considered as a damping signature of Alfvén waves (Hahn and Savin 2013).

Therefore, the first observing task (I-4-1) for the solar wind study is to diagnose the plasma properties in these regions and clarify the source regions, their contributions, and the relationships with magnetic structures. One difficulty in analyzing the source regions of the solar wind is that a longer temporal cadence (~hours) is needed to observe faint structures (such as coronal holes and AR boundaries). The throughput improvement of at least one order of magnitude by Solar-C_EUVST will allow us to approach the timescales of their evolution (a few to several minutes). Also, rolling the spacecraft by 90° will greatly reduce the scanning time for the equatorial limb observations. Regarding the relationship between the solar wind source region and magnetic field

(I-4-1), interchange reconnection between closed and open flux is widely thought to be the driver of the AR outflows. However, Hinode/EIS observations lack the spatial resolution to observe small-scale changes low down in the atmosphere at the outflow/AR boundary, and they also lack the temporal resolution to observe large-scale morphological changes that could result from reconnection at higher altitudes. The improvement in spatial and temporal resolution of Solar-C_EUVST will play a critical role in establishing which physical mechanisms are responsible for the formation and acceleration of the slow and fast wind.

To understand the acceleration mechanisms of both fast and slow solar wind, the wave dissipation rate in the corona is an important piece of information (e.g., Cranmer 2002). Therefore, the second observing task for the solar wind (I-4-2) is detecting signatures of coronal Alfvén waves in plume and inter-plume regions and measuring their energy fluxes with height. Hahn and Savin (2013) discussed a measurement of the energy carried and dissipated by Alfvén waves in a polar coronal hole using line width measurements from Hinode/EIS (Figure 5.4(b), typically V_{nt} ~ 40 km/s, which represents the Alfvén wave fluctuation amplitude). They found signatures of wave dissipation from 1.15 to 1.5 solar radii, which is consistent with previous observational estimates from SoHO/SUMER and SoHO/CDS (e.g., Banerjee et al. 1998). This dissipated energy flux possibly accelerates and heats the solar wind. Dolla & Solomon (2008) have reported similar trends in line widths observed off-limb, but they interpreted them in a different way. According to their analysis, instrumental stray light is significant for off-limb observations, and the effect needs to be taken into account when considering different heating mechanisms. To clarify the acceleration mechanisms for the solar wind, we not only need higher sensitivity spectroscopic observations to overcome the low sensitivity in faint and off-limb regions, but we also need to minimize the impact of stray light by using highly polished optical surfaces (minimal micro-roughness) and by avoiding entrance filters (that produce diffracted radiation). The improvement in spectral resolution (ex. V_{nt} ~ 4 km/s) and reducing the effect of stray light of Solar-C_EUVST will allow us to investigate more accurate energy flux for accelerating the solar wind.

Table 5.4: Summary of requirements for science objective I-4

Item	Requirement		Rationale
	I-4-1	I-4-2	
Temperature coverage (MK)	0.7~3 MK		Plumes (0.7~0.9 MK) and inter-plumes (1~1.3 MK) in coronal holes and the edges of ARs (~3 MK). Chemical abundance diagnostic capability.
Spatial resolution (arcsec)	0.8 arecsec		For distinguishing fine structures in solar wind source regions, e.g. polar plumes and inter-plumes in polar coronal holes (width ~ 10 arcsec).
Temporal resolution (s/step)	1.5 s/ 0.8"	~5 min / 0.8"	I-4-1: About or less than 1 hour scanning large FOV (280" ×280") is required, which is typical timescale of AR evolution. I-4-2: Shorter than the typical transient phenomena in polar coronal hole (e.g., jets).
FOV ($arcsec^2$)	280×280	Off limb up to 1.4 solar radii	I-4-1: The entire AR should be covered. I-4-2: Higher than 1.2 solar radii is required to quantify the wave dumping with height.
Velocity resolution (km/s)	V_d ~2 km/s V_{nt} ~ 4 km/s		To observe a few 10 km/s velocity signal. To observe height dependence for the non-thermal velocity (typically ~40 km/s).
Observation duration & total days	~1 hour 15 days each		Longer than the typical transient phenomena, such as polar coronal hole jets. Repeated measurements for statistical studies
Co-alignment	√	n/a	For co-alignment precisely with ground-based data. Simultaneous slit jaw imaging to know where the slit is located on solar images.

1": 730 km, V_d: Doppler velocity, V_{nt}: nonthermal velocity (e.g., turbulence)

II-1: Understanding of the Processes in Fast Magnetic Reconnection (Table 5.5)

The magnetic reconnection rate, how fast magnetic flux is swept through the reconnection region, predicted by standard MHD theory is much too slow to explain the rapid evolution of events observed in the solar corona. Although several theoretical models have been proposed to solve this problem (e.g., Petschek reconnection model Figure 5.5C, Plasmoid-unstable reconnection model Figure 5.5D), the physics of fast reconnection is still not clear. The solar atmosphere is one of the best space laboratories to answer this question, and observing the reconnection region (Figure 3.2A) is crucial for tackling the problem (observing task: II-1-1). Figure 5.5(A&B) show imaging observations of two flares by SDO/AIA. These images show a reconnecting current sheet structure without islands (Warren et al. 2018) and with islands (Takasao et al. 2012). However, the reconnecting current sheet cannot be seen in most flares (e.g., Figure 3.2C). Inflows (~ a few 10 km/s, Hara et al. 2011), shocks, and high-velocity jets that are expected inside the reconnection region are also not observable in most cases. The reconnection region is generally very dark while the post-flare loops are very bright. Therefore, we need high-throughput and low scatter-light observation to diagnose the reconnection region. The typical thickness of the current sheet and islands is a few arcsec, while the length is ~20". These islands and current sheets are widely observed from 171 (0.8 MK) to 195 Å (~15 MK). Thus, wide temperature coverage (wide wavelength coverage) is also important for understanding the dynamics of reconnecting current sheets and islands. Recently several papers claim that the reconnection region may not be in ionization equilibrium (e.g., Imada et al. 2011). To diagnose the non-equilibrium ionization plasma, we need a series of spectral lines from several different atomic species, for example Ca and Fe, which have different ionization timescales. Therefore, wide wavelength coverage is also very important. Typical speeds of island motions are a few hundred km/s, requiring a cadence of a few tens of seconds (15 Mm / 1000 km/s ~ 15 sec) to diagnose the reconnection region. Also, rolling the spacecraft by 90° will greatly reduce the scanning time for the limb flare region.

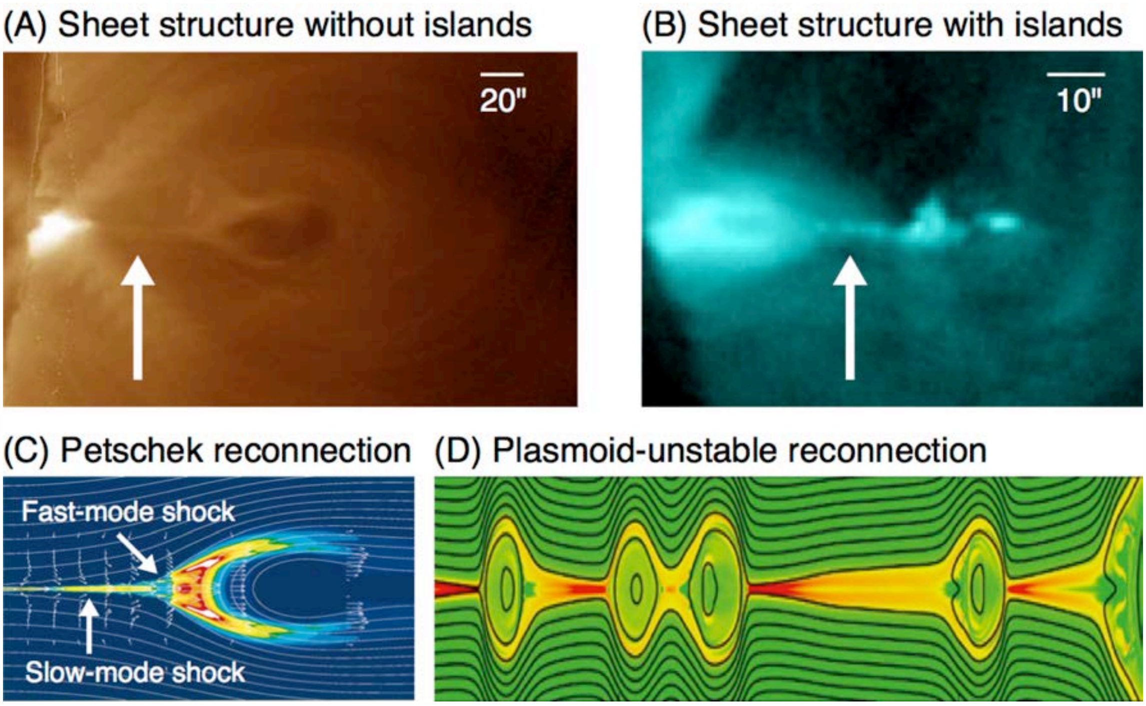

Figure 5.5: SDO/AIA observations showing a reconnecting current sheet structure (A) without islands (Warren et al. 2018) and (B) with islands (Takasao et al. 2012). Numerical simulations of magnetic reconnection (C) Petschek reconnection (Yokoyama & Shibata 1997), (D) plasmoid-unstable reconnection (Shibayama et al. 2015).

During a solar flare, thermal conduction and high-energy electrons progress down along the magnetic fields of loops and collide with the chromosphere, producing evaporation of hot plasma into the corona (e.g., Fisher et al. 1985). The chromospheric evaporation generally includes information concerning the energy conversion rate during magnetic reconnection (observing task: II-1-2). To understand the chromospheric evaporation, observations over a wide temperature range with high spatial and temporal resolution are needed since the kernels of chromospheric evaporation are small (~1") and evolve on timescales of sub-seconds (10^5 km / 10^5 km/s = 1 sec; non-thermal electron precipitation).

One of the most important Hinode findings is that magnetic reconnection events frequently occur even in the solar chromosphere (Shibata et al. 2007). Then, the key question is whether the magnetic reconnection in the chromosphere is really fast, independent of resistivity, or not. Our current guess, which is based on the Hinode observations, is “yes”. Hinode Ca II H movies, however, do not allow us to evaluate the reconnection rate (observing task: II-1-3). The time cadence of the Ca II H observations is fast enough, but quantitative measurements of e.g. flows, density, and temperature are needed to determine the reconnection rate. The typical parameters of the reconnection in the chromosphere/transition region are as follows: current sheet thickness ~1", length ~10", Alfvén velocity 100 km/s, timescale 10~100s (10" / 100 km/s), temperature 10^4~10^6 K.

Table 5.5: Summary of requirements for science objective II-1

Item	Requirement			Rationale
	II-1-1	II-1-2	II-1-3	
Temperature coverage (MK)	0.8-30	0.02-15	0.02-3	II-1-1: To observe the magnetic reconnection region where cool plasma (~1 MK) is heated up to 15 MK in the corona. Non-equilibrium ionization diagnostic capability is also important.
				II-1-2: To observe chromospheric evaporation plasma with temperatures from 0.02 (~chromosphere temperature) to 15 MK (flare temperature).
				II-1-3: To observe the magnetic reconnection region where cool plasma (~0.02 MK) is heated up to 3 MK in the chromosphere.
Spatial resolution (arcsec)	0.8			II-1-1: For resolving magnetic islands and the reconnecting current sheet during the flare (~1").
				II-1-2: For resolving kernels of chromospheric evaporation (~1").
				II-1-3: For resolving reconnecting current sheet in the chromosphere (~1").
Temporal resolution (s/step)	0.5/0.8"		1.5/0.8"	II-1-1:The scanning speed should be faster than the Alfvén speed 1000 km/s in corona, i.e. 1 sec /step in 1" step.
				II-1-2: Evolution timescale for the kernels of chromospheric evaporation (0.5 s).
				II-1-3: The scanning speed should be faster than the Alfvén speed 100 km/s in chromosphere, i.e. 7.5 s / 1" step.
FOV ($arcsec^2$)	20×280	0.8×280	20×280	II-1-1: The entire reconnection region in the corona should be observed.
				II-1-2: To observe flare ribbons evolution.
				II-1-3: The entire reconnection region in the chromosphere should be observed.
Velocity resolution (km/s)	V_d ~2 km/s			A few km/s to observe the reconnection related flows, such as reconnection inflow ~20 km/s.
Observation duration & total days	a few days 2 months each around solar maximum		~1 hour 15 days	A few days to catch at least one flare. To observe >30 events M class flare in total (Figure 4.2). Repeated measurements for statistical studies.

1": 730 km, V_d: Doppler velocity, V_{nt}: nonthermal velocity (e.g., turbulence)

II-2. Identify the Signatures of Global Energy Buildup and the Local Triggering of the Flare and Eruption (Table 5.6)

Flares and CMEs, especially stronger ones, are known to occur in ARs. In the framework of the standard flare model (Figure 3.2, e.g. Priest & Forbes 2002; Shibata & Magara 2011), a magnetic flux rope is created through the large-scale evolution of an AR, and free magnetic energy (non-potentiality) is accumulated in the atmosphere. The entire system becomes unstable and eventually the flux rope erupts, perhaps triggered by small-scale processes such as flux emergence and magnetic reconnection with the large-scale fields. Therefore, in order to understand the destabilization and eruption, we need to reveal (1) the long-term evolution of entire ARs, as well as (2) the small-scale dynamics of the flare-triggering processes.

Long-term monitoring with a large enough field of view is essential for examining the signature of energy buildup in the corona from the early stage of AR evolution. Using Hinode/EIS, Harra et al. (2009) detected an increase of 40-50 km/s in the non-thermal line widths of the Fe XII (195 Å) line a few days before the flare onset. Imada et al. (2014) also measured an upflow of 10-30 km/s one day before the flare and a loop expansion a few hours before (see Figure 5.6), both in the Fe XII (195 Å) line. However, the physical origin of these pre-flare phenomena and their relationship with the global energy buildup remain unclear. To this end, Solar-C_EUVST will conduct monitoring of entire ARs (field of view of e.g. 280"×280") for their full disk passage (up to 2 weeks) and, through the investigation of multiple spectral lines and comparison with photospheric evolution (observing task: II-2-1), it will reveal how and where these upflows originate. To resolve the Doppler flows in the lower atmosphere (e.g. chromosphere), where the sound speed is a few 10 km/s, a velocity resolution of ~2 km/s is needed.

Observations have revealed that flares are often associated with small-scale, newly-emerging magnetic flux and its trigger interaction with pre-existing fields (e.g. Feynman & Martin 1995; Wang & Sheeley 1999). Photospheric observations (e.g. Toriumi et al. 2013; Bamba et al. 2013) show that the triggering systems have spatial scales of 5"-20" (Bamba & Kusano 2018), and often exhibit pre-flare brightenings in the chromosphere that probably indicate local reconnection with the pre-existing fields. Since the dynamics of the trigger fields is determined by the Alfvén speed (a few 10 km/s), the evolution time scales should be less than 10 minutes. To quantify the trigger dynamics, Solar-C_EUVST will perform repeated scanning around the polarity inversion lines with medium spatial and temporal resolution (~1" and ~1 minute, respectively), simultaneously from the chromosphere to the upper atmosphere, and measure the flow fields (observing task:II-2-2). We will identify the MHD instability modes by directly comparing the observational results with magnetic measurements in the photosphere and numerical simulations. Understanding the flare trigger is crucial for realizing flare predictions.

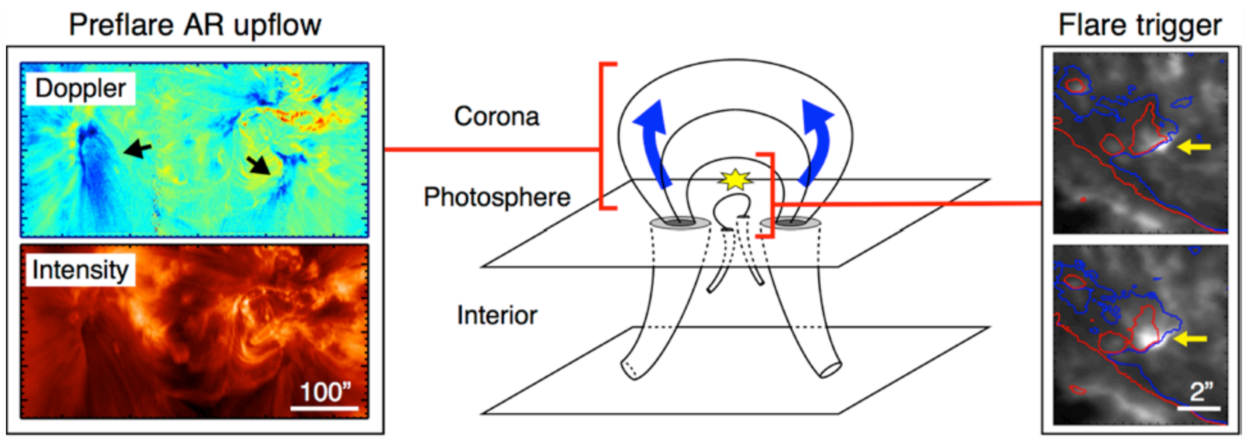

Figure 5.6: (Left) Preflare AR upflow observed by Hinode/EIS (Imada et al. 2014). Blue and red in the Dopplergram indicate upflow and downflow, respectively. (Right) Local flare-triggering fields with small-scale reconnection (arrows) obtained by Hinode/SOT (Toriumi et al. 2013).

Table 5.6: Summary of requirements for science objective II-2

Item	Requirement		Rationale
	II-2-1	II-2-2	
Temperature coverage (MK)	0.02-10	0.02-1	II-2-1: A broad temperature range should be covered to monitor pre-flare phenomena.
			II-2-2: Lower temperature ranges should be covered to reveal the dynamics of the lower atmosphere.
Spatial resolution (arcsec)	1.6	0.8	II-2-1: Resolution should be better than or similar to AIA (~1.6") is needed.
			II-2-2: High resolution observations should be conducted to resolve the flare-triggering fields (~1").
Temporal resolution (s/step)	0.5/1.6"	1.5/0.8"	II-2-1: About or less than 1 hour scanning large FOV (280"x280") is required, which is the typical timescale of active region evolution. Constant, continuous monitoring is crucial for this observation.
			II-2-2: Less than 10 minutes for the monitoring of a small FOV (20"×280") to track the evolution of the flare triggering region, and preferably about or less than 1 minute during the flaring phase.
FOV ($arcsec^2$)	280×280	20×280	II-2-1: The entire AR should be covered.
			II-2-2: To observe flare triggering region.
Velocity resolution (km/s)	$V_d \sim 2$ $V_{nt} \sim 5$	$V_d \sim 2$	II-2-1: For the coronal measurements, a few km/s for the Doppler velocity and ~10 km/s for the turbulence velocity are required to resolve, for example, the pre-flare dynamics and non-thermal broadening.
			II-2-2: For the chromospheric measurements, ~2 km/s for the Doppler velocity is desirable so that the Alfvén and acoustic velocities (a few 10 km/s) are resolved.
Observation duration & total days	a few days 1 month each		A few days are requested to catch at least one flare event (up to 2 weeks for the whole disk passage). To observe >15 events M class flare in total (Figure 4.2).
Co-alignment	n/a	√	For precise co-alignment with ground-based data. Simultaneous slit jaw imaging to know where the slit is located on solar images.

1": 730 km, V_d: Doppler velocity, V_{nt}: nonthermal velocity (e.g., turbulence)

6. Instrumentation of the mission [5-2–1]
ミッションで使用する装置

6.1. One sentence description of the technology to realize the investigations [5-2-1]
実施する実験・観測・分析などを実現する技術(1文で記述すること)

The proposed mission carries a UV imaging spectroscopic telescope that has broad passbands in 170 – 1280 Å with high spatial resolution of 0.4″, high throughput that achieve a high temporal resolution of 0.5 s, and high spectral resolution to resolve velocity fluctuations of 2 km/s.

6.2. Comparisons of the selected technology with other technologies [5-2-2]
実施する実験・観測・分析などを実現する方法・技術について，他の技術，および類似技術との比較

In this subsection, first we compare possible technologies for the coronal observations from the viewpoint of observation parameters, and determine the best technology to achieve our science objectives. Second, we examine wavelength bands and spectral lines for the selected technology. Third we examine the radiometric performance of the chosen wavelength bands to confirm the capability of plasma diagnostics for our science objectives. Fourth, we confirm the photometric accuracy for the selected technology whether it satisfies our scientific requirements. After that we compare the other missions that have similar technologies to that of the proposed mission.

6.2.1 Comparison of technologies for coronal observations

Table 6.1: Comparison of possible technologies. Yellow filled cells show the parameters that satisfy our scientific requirements.

	UV imaging spectroscopy (selected technology)	UV imaging	SXR imaging spectroscopy (micro-calorimeter)	SXR imaging spectroscopy (CMOS)	SXR imaging	Visible spectroscopy with coronagraph
Temporal resolution (exposure) [s]	0.1-1	~1	<1	<10	<10	0.25
Spatial resolution [″]	0.4	1.6 (AIA) 0.2 (Hi-C)	~1	1	1	~10
Spectral resolution [λ/dλ]	~5000	N/A	~1000	5	N/A	~10000
Temperature coverage [K]	20k – 15M	6k – 15M	6M - 50M	> 5M	1.3M – 32M	10k, 1.5-2.5M
Temperature resolution [d(logT[K])]	0.05-0.1	0.2-0.8	0.1	0.1	0.2	N/A
Field of view [″]	300	full disk (AIA) 400 (Hi-C)	~1000	<500	Full disk	>2.8R_sun, only off-limb

References:
UV imaging: SDO/AIA (Lemen et al. 2012), Hi-C (Cirtain et al. 2013)
SXR imaging spectroscopy (microcalorimeter): Prototype TES X-ray microcalorimeter array (Christe et al. 2016)
SXR imaging spectroscopy (photon counting with CMOS): PhoENiX (Sakao et al. 2014)
SXR imaging: Hinode/XRT (Golub et al. 2007)
Visible spectroscopy with coronagraph: NSO/COMP (Tomczyk et al. 2008)

The proposed technology should be the best method to obtain the data described in Tables 5.1 – 5.5. Table 6.1 compares typical observation parameters obtained by different technologies for coronal observations. All technologies in the table satisfy our scientific requirement of the temporal resolution, and especially UV and soft x-ray (SXR) technologies satisfy the requirement of the field of view. UV technologies have a better spatial resolution, and meet the science objectives to observe a wide temperature range from the upper chromosphere to the corona seamlessly and simultaneously. UV spectroscopic and visible coronagraphic technologies have a capability to resolve the required velocity structures. Therefore, we conclude that UV spectroscopic technologies are the best for the science objectives described in the previous sections.

6.2.2 Temperature coverage of UV lines and spectral line selection

The observations must cover all relevant temperatures and structures to reveal the energy flows and energy release signatures throughout the atmosphere. Tracking structures and flows through different temperature regimes at 0.4″ resolution requires strict co-alignment of all spectral bands. Thus, a unique optical path to the grating assembly is a fundamental requirement and design driver. It is equally important to explore solar plasma at high temperatures above 5 MK. If the corona is heated impulsively by numerous small-scale impulsive events, they are predicted to produce hot plasma above 5 MK. Spectral lines from ions such as Fe XVIII (7.1 MK) or ions formed at higher temperatures can constrain the nanoflare heating scenario. Highly ionized iron ions, i.e., Fe XVIII through Fe XXIV, also allow us to explore the temperature evolution for out of ionization equilibrium plasma and therefore give new insights into the reconnection region.

UV chromospheric lines of the hydrogen Lyman series (20 kK) are located between 925 – 1085 Å. Strong chromospheric lines such as N I and the strongest hydrogen line, Ly-alpha 1216 Å, are distributed between 1115 – 1275 Å. To observe continuously through the upper chromosphere to the lower transition region, O II – O IV (0.05 – 0.16 MK) lines located between 690 – 850 Å are crucial. Lines formed between the upper transition region and the lower corona such as O V (0.25 MK) and Ne V – Ne VII (0.32 – 0.63 MK) are located between 463 – 637 Å. Intense lines formed in the lower corona are located between 170 – 215 Å, which are confirmed by the Hinode/EIS observations. High temperature AR lines such as Fe XVIII 975 Å (7.1 MK) were a missing window of the Hinode/EIS observations. Such observations can be achieved at the same time by observing the passband 925 – 1085 Å. High temperature coronal emission from Fe XX – Fe XXII is also located between 690 – 850 Å. Therefore, the required temperature coverage resulted in the careful selection of the six spectral passbands, which consist of one short-wavelength (SW) band and five long-wavelength (LW) bands as shown in Figure 6.1. Note that two of the LW bands are taken by second order diffraction.

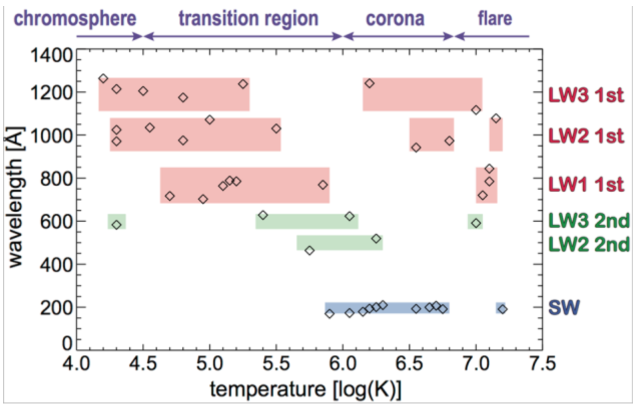

Figure 6.1: Selected spectral passbands and temperature coverages. Strong lines are marked as diamond symbols.

The key requirement for the instrument is to make measurements with spectral lines formed over the entire solar atmosphere, i.e., at chromospheric, transition region, corona and flare temperatures with high spatial and temporal resolutions. This requires bright lines at all temperatures and has led to the selection of the six spectral bands. The brightest spectral lines in the passband are marked in Figure 6.1 and listed in Table 6.2. Note that a vastly larger number of fainter lines observed by EIS and SUMER are not marked but locate in the filled regions.

Table 6.2: List of the brightest lines to be observed with Solar-C_EUVST. Green, blue, pink, yellow, and light blue show lines formed in the chromosphere, upper transition region, lower transition region, corona, and flaring region.

Ion	Wavelength [Å]	Log T [K]	Radiance [erg/s·cm^2·sr]			Channel (order)
			QS	AR	Flare (GOES C1.1)	
H_2	1163.85	3.60	—	193[a]	—	LW-3
Si II	1264.74 (2 lines)	4.20	149[b]	480[b]	>AR	LW-3
H I	1215.67	4.30	65000[b]	220000[b]	>AR	LW-3
H I	1025.72	4.30	793[a]	6253[b]	>AR	LW-2
H I	972.58	4.30	139[a]	1452[b]	>AR	LW-2
He I	584.34	4.30	580[b]	5080[b]	140000[g]	LW-3 (2)
Si III	1206.502	4.50	695[b]	3560[b]	74000[h]	LW-3
C II	1036.340	4.55	40[a]	290[b]	1690[h]	LW-2
O II	718.506 (2 lines)	4.70	9.8[a]	40[a]	2229[h]	LW-1
C III	977.020	4.80	804[a]	3666[b]	58700[h]	LW-2
C III	1176.0 (6 lines)	4.80	221[c]	823[d]	21310[h]	LW-3
O III	703.854	4.95	30[a]	123[a]	4380[h]	LW-1
S IV	1072.974	5.00	5.5[c]	26[a]	434[h]	LW-2
N IV	765.147	5.10	67[a]	142[a]	5750[h]	LW-1
O IV	790.199 (2 lines)	5.15	83[b]	184[b]	8900[h]	LW-1
S V	786.470	5.20	27[c]	61[d]	1760[h]	LW-1
N V	1238.823	5.25	61[b]	549[b]	1130[h]	LW-3
O V	629.732	5.40	335[b]	1019[b]	90900[g]	LW-3 (2)
O VI	1031.914	5.50	328[a]	2460[b]	8110[h]	LW-2
Ne VII	465.22	5.75	120[b]	989[b]	4760[h]	LW-2 (2)
Ne VIII	770.428	5.85	54[b]	600[b]	3170[h]	LW-1
Fe IX	171.073	5.90	892[c]	8400[d]	30600[h]	SW
Fe X	174.531	6.05	406[c]	5320[d]	16300[h]	SW
Mg X	624.962	6.05	51[b]	398[b]	4190[h]	LW-3 (2)
Fe XI	180.408	6.15	251[c]	4380[d]	13300[h]	SW
Fe XII	195.119	6.20	174[c]	3890[d]	12300[h]	SW
Fe XII	1241.950	6.20	3.7[c]	79[d]	247[h]	LW-3
Fe XIII	202.044	6.25	41[c]	1248[e]	3960[h]	SW
Si XII	520.666	6.25	22[c]	1130[f]	6790[h]	LW-2 (2)
Fe XIV	211.317	6.30	73[c]	1720[f]	10500[h]	SW
Ca XIV	193.974	6.55	—	312[e]	766[h]	SW
Ca XIV	943.587	6.55	—	7.3[f]	18[h]	LW-2
Ca XV	200.972	6.65	—	239[e]	751[h]	SW
Ca XVI	208.604	6.70	—	122[e]	946[h]	SW
Ca XVII	192.858	6.75	—	147[e]	3780[h]	SW
Fe XVIII	974.860	6.80	—	88[f]	2500[h]	LW-2
Fe XIX	592.236	7.00	—	9.3[f]	1530[h]	LW-3 (2)
Fe XIX	1118.07	7.00	—	8.6[f]	1500[h]	LW-3
Fe XX	721.559	7.05	—	—	1580[h]	LW-1
Fe XXI	786.162	7.10	—	—	178[h]	LW-1
Fe XXII	845.57	7.10	—	—	2180[h]	LW-1
Fe XXIII	1079.414	7.15	—	—	205[h]	LW-2
Fe XXIV	192.03	7.20	—	—	18100[h]	SW

(a) From SUMER spectra. The active region (AR) values are from a modest one.
(b) Vernazza and Reeves, 1978, ApJS 37, 485.
(c) CHIANTI 7.0 (CHIANTI ionization equilibria and coronal abundances, density=5×10^9 cm^{-3}, quiet Sun DEM).
(d) CHIANTI 7.0 (CHIANTI ionization equilibria and coronal abundances, density=5×10^9 cm^{-3}, active region DEM).
(e) Warren et al., 2011, ApJ 734, 90.
(f) CHIANTI 7.0 (CHIANTI ionization equilibria and coronal abundances, density=5×10^9 cm^{-3}, active region core DEM from Warren et al. 2011).
(g) From CDS spectra of a GOES C1.1 flare.
(h) CHIANTI 7.0 (CHIANTI ionization equilibria and coronal abundances, density=5×10^9 cm^{-3}, DEM from CDS spectra of a GOES C1.1 flare).

6.2.3 Radiometric performances to achieve high-throughput optics

The instrument must achieve high throughput performance. The effective area (EA) in cm^2 is related to the radiance, L, in erg/s·cm^2·sr by the following formula:

$$EA = 8.3 \times 10^2 \frac{N}{L t_{exp} \lambda} \ [\mathrm{cm}^2] \,,$$

where N is photon number, t_{exp} is exposure time in second, and λ is wavelength in Å. EA as a function of wavelength was calculated and is given in Figure 6.2(a) for SW and LW bands based on the EAs of Hinode/EIS and SoHO/SUMER, respectively. The EA of the SW band is calculated under the assumption that the diameter of the primary mirror is twice as large as Hinode/EIS and the visible-IR filter in the optical path is removed. The EAs of LW bands are calculated under the assumption that the number of reflections is reduced from 3 to 1 and the diameter of the primary mirror increases from 12 cm to 28 cm. The calculation includes the mirror, grating and detector efficiencies, as well as the relevant geometrical factors (i.e., mirror area and the splitting of the grating into the SW and LW channels). The plot includes, for comparison, the published effective areas of Hinode/EIS, SoHO/SUMER and SoHO/CDS. The peak efficiencies give a factor of ≈ 10 improvement with respect to Hinode/EIS in the EUV and an improvement of a factor of ≈ 40 over SoHO/SUMER in the FUV. Figure 6.2(b) shows the expected signal (in count/arcsec^2) obtained by multiplying the EA by the radiances for different solar regions and by considering typical exposure times for those regions and a resolution element of 1 arcsec^2.

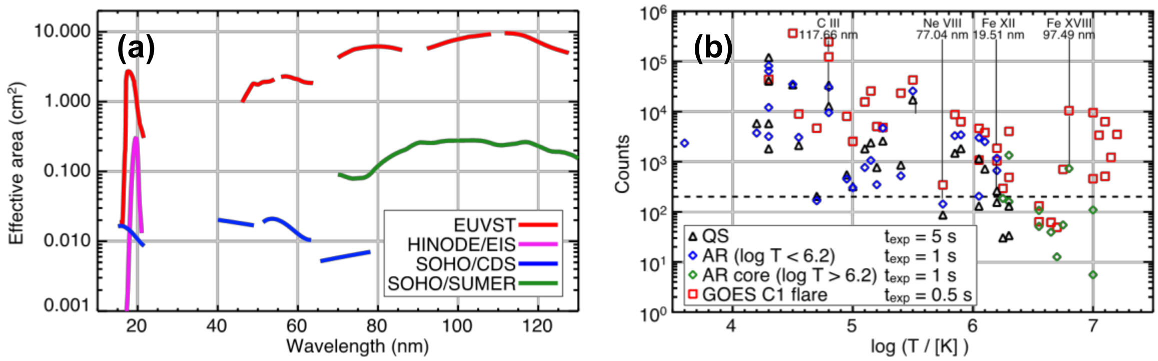

Figure 6.2: (a) Assumed Solar-C_EUVST effective area based on the baseline architectures described in section 15. The effective areas of Hinode/EIS, SoHO/SUMER, and SoHO/CDS are also shown for comparison. (b) Expected count rates (count/arcsec^2) for the indicated exposure times for different solar observational targets (5 s for the quiet Sun, 1 s for active regions, and 0.5 s for a small flare). The horizontal dashed line marks the 200 counts (in the spectral line) level necessary to determine line positions with a ≤ 2 km/s accuracy as shown in section 6.2.4.

6.2.4 Photometric accuracy

Spectroscopic observations are challenging because they distribute the observed emission into many small spectral bins. Furthermore, spectroscopic plasma diagnostics often rely on high-order moments of the line profile or on information from multiple lines. To evaluate the diagnostics of interest we have performed Monte Carlo simulations where we assume a total line intensity, Doppler shift, non-thermal velocity, and background and generate a random realization of the line profile. We then infer the values of these parameters from a least-squares fit to the synthetic data, just as we will for the actual observations. Repeating this process for different intensity levels allows us to estimate how the uncertainties in the diagnostics depend on the observed counts.

An example calculation is shown in Figure 6.3. Here we have simulated the C III 977.02 Å line assuming no Doppler shift, a non-thermal velocity of 30 km/s, a dispersion of 37 mÅ per spectral pixel, an instrumental broadening (full width at half maximum; FWHM) of 2.5 pixels, and a background level of 2.5 counts per spectral bin. This simulation indicates, as one would expect, that approximately 100 total counts in the line profile are needed to measure the intensity to 10%. An error of 2 km/s in the Doppler shift is achieved for approximately 200 total counts. Approximately 150 counts are needed to achieve an uncertainty of 15% in the non-thermal velocity. Finally, we have also estimated the uncertainty in the electron density, which is derived from the ratio of two lines, as a function of total counts. Here we use the Fe XII 186.867/195.119 Å ratio to illustrate this. About 700 counts are needed to measure the electron density to 30%. Note that the needed count levels depend strongly on the line width. Lines formed at higher temperatures will have a larger thermal component in the width and require more counts to achieve the same level of accuracy in the Doppler shift and non-thermal velocity.

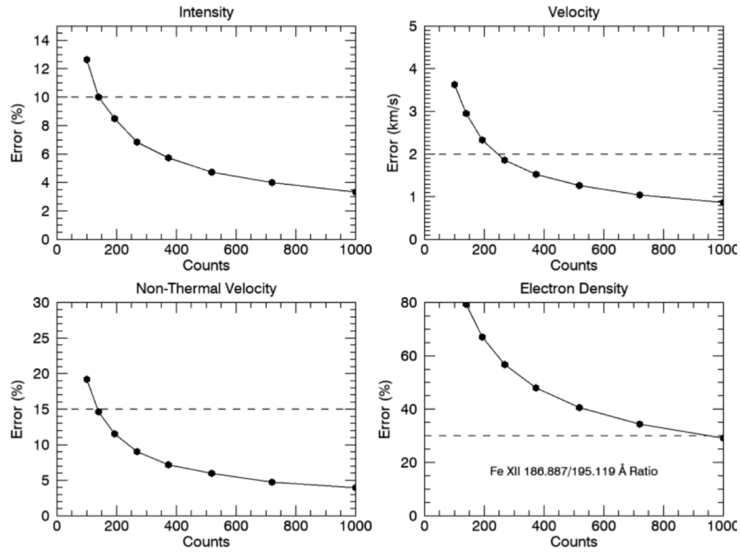

Figure 6.3: Errors in the moments of a line profile as a function of total counts. For the electron density the counts are those for the weaker line.

Another source of uncertainty in the plasma diagnostics is the instrument calibration. Of primary concern to Solar-C_EUVST is the relative calibration, which impacts the use of diagnostics formed from emission observed at different wavelengths. Solar-C_EUVST will have a relative calibration of 25% over all wavelengths. This would increase the uncertainty in the density to a factor of 4 (0.6 in the log) for lines widely separated in wavelength. However, for lines close in wavelength the relative uncertainty in the calibration will generally be much less and the uncertainty will be lower.

6.2.5 Comparison with other UV spectroscopic instruments

Observation performances of current and forthcoming coronal UV spectrometers introduced in Section 3.3 are compared in Table 6.3. The enormous number of spectral lines with high spatial and temporal resolutions recorded by Solar-C_EUVST will allow determination of the thermodynamic state of the plasma (density, temperature) and its chemical composition at all temperatures. Observations of this completeness are unprecedented.

6.3. Major flight / ground trades [6-3-3] 搭載機器/地上系の主要な機能分担の検討

Table 6.4 gives the results from our conceptual study. The study suggests that the following items shall be studied in more details in the design phase:

- The best method to capture large flares with a rather narrow field of view instrument is semi real-time pointing adjustment operations. The baseline method will be to follow that used in Hinode's flare watch operations which allows for such last-minute pointing adjustment.
- The amount of data will increase during flare campaigns because of the inherently unpredictable nature of flare onset. Appropriate methods for storing and downloading flare data volumes will be studied.

Table 6.3: Solar-C_EUVST performance in comparison with current and forthcoming spectrometers. Yellow filled cells show the specifications that meet our observation target.

	Existing mission			Mission Under Study		
	Hinode/ EIS	SoHO/ SUMER	IRIS	Solar Orbiter/ SPICE	MUSE	**Solar-C_ EUVST**
Temporal resolution for a slit position (1)	10 – 60 s for AR 20 – 120 s for QS	≥15 – 60 s (2)	<10 s for AR 10 s for QS	5 s	1.0 s for AR 0.1 s for flare	0.2(4) – 5 s for AR 0.2 – 20 s for QS
Spatial resolution (1″=725 km on the Sun)	2″ – 3″	1.5″	0.33″	1″	0.4″	0.4″
Field of View (without repointing)	±290″×512″	±1920″×300″	32″×120″	960″x240″	170″x170″	±150″×280″
Wavelength bands [Å]	170 – 210 250 – 290	500 – 1600	1332 – 1358 1389 – 1407 2783 – 2835	702 – 792 972 – 1050 485 – 525	107 – 109 170 – 174 276 – 288	170 – 215 463 – 542 557 – 637 690 – 850 925 – 1085 1115 – 1275
Primary temperature coverage ($\log_{10} T$/[K])	4.9, 5.6 – 7.2	3.6 – 5.8, 6.8 – 7.0(3)	3.7 – 5.2, 7.0	3.6 – 5.8, 6.8 – 7.0	5.9, 6.4, 7.0-7.1	4.2 – 7.2
Diagnostics capabilities	LOS Velocity Electron Density Electron/ion Temperature DEM	LOS Velocity Electron Density Electron Temperature	LOS velocity	LOS Velocity Electron Density Electron/ion Temperature	LOS velocity	LOS Velocity Electron Density Electron/ion Temperature DEM

(1) The values given here are typical exposure duration for multiple numbers of spectral lines covering a wide temperature range.

(2) There are several lines in the SoHO/SUMER range that could actually be recorded at higher cadence even on the quiet Sun but there is neither sufficient telemetry nor on-board storage to allow this. Values given here refer to the time required to transmit just one window of 50×300 pixels (300″slit). None of these problems will affect Solar-C_EUVST.

(3) SoHO/SUMER can record spectral lines in only one spectral window of ≈40 Å at a time. If spectral lines in another spectral window are measured, the spectral window must be changed before the exposure.

(4) Exposure time and time step of 0.2 s is for one line per camera (4 spectral lines).

6.4. Data to be returned in the course of the investigation (= mission data): telemetry data, sample data etc. [2-2-1] ミッションで獲得するデータ, テレメトリーデータ，サンプルなど (以下ミッションデータ)

This section describes the data to be returned from the proposed mission instrument. Typical examples of observing sequences required for achieving each science objective are shown in section 6.4.1 to define the observing modes and estimate the amount of data, followed by the requirement for telemetry data in section 6.4.2 and the expected data analysis in section 6.4.3.

Table 6.4: Flight and ground trades

Item	Results from conceptual study
Decision of the observation target and the timeline	• Decided and confirmed by observers in the daily meeting. The observers monitor solar activities by using full disk images provided by other ground-based/space-bone telescopes. Once the targets are confirmed, observers make a timeline and decide observation sequences for each target. The decided observation plans are uploaded to the satellite. This is what has been done in Hinode daily operations.
Handling the large amount of the data from observations	• The data downlink capability may be insufficient to download the larger amount of the data to the ground. • Depending on scientific target, observers choose the detector areas that include the appropriate bright lines and the size of the field of view during the planning of the observations. Thus, only parts of the detector areas are downloaded.
Onboard processes	• Lossy and lossless compressions of the observed data are performed in the onboard processor • Higher order data products (e.g. intensity, velocity, line width) will not be derived onboard. This is the same as Hinode.
Observations of transient phenomena	• To increase chances to observe transient phenomena, semi-real-time pointing adjustment operations or large data memory should be installed. • The semi-real-time pointing adjustment will be performed manually by the ground operation. • An onboard function may be required to protect the science data when large flares occur. • To confirm preserved data to be downloaded, thumbnail images are provided to the ground operation.
Estimation of the orbital variation of the wavelength shifts	• By deriving relative wavelength among lines emitted from the same ion species, the shift can be calibrated in the data analysis on the ground. The wavelength shift is typically ± 6 km/s in the case of a sun synchronous orbit.
Calibration of wavelength drift due to the temperature variations	• An artificial neural network is incorporated to establish a relationship between the instrumental temperatures and the spectral drift. The same method has been used for the Hinode/EIS wavelength calibration (Kamio et al. 2010).
Adjustment of the focus position	• The best focus position is evaluated in the initial phase of the flight by analyzing data taken at several focus positions on the ground. • Focus mechanisms are required to be onboard based on the tolerances required for the optics optimum performance. • The opt-mechanical design should be taken so that the focus change is negligible for the orbital variation.
Radiometric calibration	• Radiometric calibration is performed by using an internationally recognized source on the ground.

6.4.1 Required observations

One way to think about the design requirements for the telemetry data is to devise a set of basic observing modes that can be used singularly or in combinations (observing sequences or programs) to achieve the instrument and mission science objectives. Table 6.5 provides typical examples of the programs (observing sequences) expected to be used for each of the science objectives. The table also gives an estimate of the duration of one observation required for each study, and the data volume produced by each study when the study is run in the duration.

The basic observing modes used to form the studies described in Table 6.5 are listed in Table 6.6. Collectively, they define the design requirements for the instrument. The estimated Solar-C_EUVST data rate production of each observing program and mode is given in Tables 6.5 and 6.6, respectively.

Table 6.5: Required observing sequences (programs).

Science sub-objective	Tasks of observations	Observing sequences	Duration / Data volume	Data rate [Mbps]
I-1: Nanoflares	I-1-1:	1) AR-Context × 1 2) AR-High_S&S × 100 Repeat 1) & 2) × 9	87.5 s / 0.11 Gb 300 s / 0.17 Gb 3487.5 s / 2.52 Gb	0.72
	I-1-2:	1) AR-Context × 1 2) AR-High_S&S × 100 Repeat 1) & 2) × 9	87.5 s / 0.11 Gb 300 s / 0.17 Gb 3487.5 s / 2.52 Gb	0.72
	I-1-3:	1) AR-Context × 1 2) AR-High_Small × 1 3) AR-Mid_Small × 14 Repeat 2) & 3) × 4	87.5 s / 0.11 Gb 250 s / 0.06 Gb 525 s / 0.31 Gb 3187.5 s / 1.92 Gb	0.60
	I-1-4:	1) AR-Context × 1 2) AR-Mid_Small × 14 Repeat 1) & 2) × 6	87.5 s / 0.11 Gb 525 s / 0.31 Gb 3675 s / 2.52 Gb	0.69
I-2: Wave	I-2-1:	1) AR-Context × 40 2) AR-Mid_Small × 96 1) or 2) × 1	3500 s / 4.12 Gb 3600 s / 2.12 Gb 3500 (3600) s / 4.12 (2.12) Gb	1.18 (0.59)
	I-2-2:	1) AR-Context × 1 2) AR-High_S&S × 100 Repeat 1) & 2) × 9	87.5 s / 0.11 Gb 300 s / 0.17 Gb 3487.5 s / 2.52 Gb	0.72
	I-2-3:	1) AR-Context × 1 2) AR-High_Small × 4 Repeat 1) & 2) × 5	87.5 s / 0.11 Gb 1000 s / 0.25 Gb 5437.5 s / 1.8 Gb	0.33
I-3: Spicules	I-3-1:	1) QS-Context × 1 2) AR-High_SSmall × 25 Repeat 1) & 2) × 2	262.5 s / 0.21 Gb 1250 s / 0.88 Gb 3025 s / 2.18 Gb	0.72
	I-3-2:	1) QS-Context × 1 2) AR-High_SSmall × 25 Repeat 1) & 2) × 2	262.5 s / 0.21 Gb 1250 s / 0.88 Gb 3025 s / 2.18 Gb	0.72
I-4: Solar Wind	I-4-1:	1) AR-Context × 1 2) AR-Mid_Full × 2 Repeat 1) & 2) × 3	87.5 s / 0.11 Gb 1050 s / 0.62 Gb 3412.5 s / 2.19 Gb	0.64
	I-4-2:	1) QS-Context × 1 2) QS-Low_S&S_L × 1 3) QS-Low_Small_L × 4 Repeat 1) & 2) & 3) × 2	262.5 s / 0.21 Gb 300 s / 0.01 Gb 1200 s / 0.05 Gb 3520 s / 0.54 Gb	0.15
II-1: Fast Magnetic Reconnection	II-1-1:	1) AR-Context × 1 2) FL-Mid_Full × 4 3) FL-Mid_Small × 56 4) FL-Mid_S&S × 1400 Repeat 1) & 2) × 240 Repeat 1) & 3) × 240 Repeat 1) & 4) × 240	87.5 s / 0.11 Gb 700 s / 1.23 Gb 700 s / 1.23 Gb 700 s / 0.62 Gb 2 days / 322 Gb 2 days / 322 Gb 2 days / 175 Gb	1.87 1.87 1.01
	II-1-2:	1) AR-Context × 1 2) FL-Mid_Small × 56 3) FL-Mid_S&S × 1400 Repeat 1) & 2) × 240 Repeat 1) & 3) × 240	87.5 s / 0.11 Gb 700 s / 1.23 Gb 700 s / 0.62 Gb 2 days / 322 Gb 2 days / 175 Gb	1.87 1.01
	II-1-3:	1) QS-Context × 1 2) AR-Mid_Small × 14 Repeat 1) & 2) × 4	262.5 s / 0.21 Gb 525 s / 0.31 Gb 3150 s / 2.08 Gb	0.66
II-2: Flare trigger	II-2-1:	1) AR-Context × 1 Repeat 1) every 30 min 336 times	87.5 s / 0.11 Gb 1 week / 36.96 Gb	0.06
	II-2-2:	1) AR-Context × 1 2) AR-Mid_Small × 30 Repeat 1) & 2) × 144	87.5 s / 0.11 Gb 1125 s / 0.66 Gb 2 days / 111 Gb	0.64

Table 6.6. Observing modes

	Obs. mode	FOV	Slit width / exposure	Step size	Cadence	T range	N° lines	Data rate[(1)]
1	QS-Context	280″×280″	1.6″ (1.5 s)	1.6″	262.5 s	0.03 – 1.5 MK	16	0.78 Mbps
2	QS-High_Full	100″×100″	0.40″ (15 s)	0.40″	3750 s	0.03 – 1.5 MK	8	0.06 Mbps
3	QS-High_Small	20″×100″	0.40″ (15 s)	0.40″	750 s	0.03 – 1.5 MK	8	0.06 Mbps
4	QS-Mid_Full	100″×100″	0.80″ (5 s)	0.80″	1750 s	0.03 – 1.5 MK	8	0.24 Mbps
5	QS-Mid_Small	20″×280″	0.80″ (5 s)	0.80″	125 s	0.03 – 1.5 MK	8	0.24 Mbps
6	QS-High_S&S	0.4″×100″	0.40″ (9 s)	0.40″	9 s	0.03 – 15 MK	8	0.09 Mbps
7	QS-Mid_S&S	0.8″×140″	0.80″ (5 s)	0.80″	5 s	0.03 – 15 MK	8	0.12 Mbps
8	QS-Low_S&S_L	0.8″×280″	0.8″ (300 s)	0.8″	300 s	0.03 – 15 MK	16	0.01 Mbps
9	QS-Low_Small_L	16″×280″	1.6″ (30 s)	1.6″	300 s	0.03 – 15 MK	16	0.04 Mbps
10	AR-Context*	280″×280″	1.6″ (0.5 s)	1.6″	87.5 s	0.03 – 15 MK	16	1.18 Mbps
11	AR-High_Full	100″×100″	0.40″ (5 s)	0.40″	1250 s	0.03 – 15 MK	12	0.25 Mbps
12	AR-High_Small	20″×100″	0.40″ (5 s)	0.40″	250 s	0.03 – 15 MK	12	0.25 Mbps
13	AR-High_SSmall	10″×100″	0.40″ (2 s)	0.40″	50 s	0.03 – 15 MK	12	0.63 Mbps
14	AR-Mid_Full*	280″×280″	0.80″ (1.5 s)	0.80″	525 s	0.03 – 15 MK	12	0.59 Mbps
15	AR-Mid_Small*	20″×280″	0.80″ (1.5 s)	0.80″	37.5 s	0.03 – 15 MK	12	0.59 Mbps
16	AR-High_S&S	0.4″×100″	0.40″ (3 s)	0.40″	3 s	0.03 – 15 MK	16	0.56 Mbps
17	AR-Mid_S&S	0.8″×140″	0.80″ (1.5 s)	0.80″	1.5 s	0.03 – 15 MK	16	0.78 Mbps
18	FL-Mid_Full*	280″×280″	0.80″ (0.5 s)	0.80″	175 s	0.03 – 15 MK	12	1.76 Mbps
19	FL-Mid_Small*	20″×280″	0.80″ (0.5 s)	0.80″	12.5 s	0.03 – 15 MK	12	1.76 Mbps
20	FL-Mid_S&S*	0.8″×140″	0.80″ (0.5 s)	0.80″	0.5 s	0.03 – 15 MK	12	0.88 Mbps
21	Slit camera monitor[(2)]	30″×150″	(0.2 s)	n/a	7s	0.01 MK	n/a	0.06 Mbps[(3)]

(1) Based on 60 pixel wide windows. The number of pixels along the slit is given by the y-size of the FOV divided by the slit width (spatial binning equal to resolution across slit). 14 bits/pixel and lossless compression (factor 2) are assumed. Note that lossless compression of EIS is ~35%, largely depending on the features in the data. We assume lossy compression (factor 4) in the case of flare and some AR study, marked *.

(2) Solar-C_EUVST context and Slit camera monitor images are also needed to facilitate alignment with other observations (e.g., DKIST).

(3) Compression to 2.2 bits/pixel is assumed.

6.4.2 Telemetry and onboard data recorder requirements

Solar-C_EUVST's broad temperature coverage (multiple lines to be recorded simultaneously) at high temporal resolution requires an adequate telemetry rate to ensure operations. According to Table 6.5, the data rates expected from each observing program of most tasks are up to 0.72 Mbps. The typical duration of each observing program in Table 6.5 is about 1 hour, and a variety of observing programs run during the daily observations to optimize the science return as described in section 11. Thus, when observations are carried out continuously without idle periods, an average data rate during the observations is about 0.72 Mbps in the most programs. This is the minimum requirement for the data rate. If a lower data rate is required due to restrictions on the telemetry resource in some periods, idle times will be imposed between two consecutive observing programs.

A data recorder is required to store the science data from the instrument, because continuous contacts with ground stations for 24 hours are unlikely (trade-off study in section 14.2 (6)). Moreover, Tasks I-2-1, II-1-1, and II-1-2 require higher data rates of 1.18, 1.87, and 1.87 Mbps, respectively. Science data obtained at these data rates should be stored adequately in the memory of the onboard data recorder. For Task I-2-1, a volume for storing the produced data, 4.12 Gbits (1.18 Mbps × 1 hour), is required in the data recorder. Regarding the flare-related observations of Tasks II-1-1 and II-1-2, it is desirable to continuously run the defined observing programs as long as possible since the prediction of flare occurrence is difficult. The continuous observations will produce 162 Gbits in a day (1.87 Mbps × 24 hours). However, data that are truly necessary for achieving Tasks II-1-1 and II-1-2 are obtained typically within 3 hours around the onset of the flare, and the amount of the data is 20 Gbits (1.87 Mbpts × 3 hours). Therefore, 20 Gbits is the minimum requirement for the data recorder volume.

Note that, as listed in section 6.3, an onboard function to protect flare data from being overwritten or a quick-look browser before data downloading would be required.

In summary, the minimum requirements of the data rate and the volume of the onboard data recorder are 0.72 Mbps and 20 Gbits, respectively.

6.4.3 Usage of the data

From the spectroscopic data obtained by Solar-C_EUVST, various plasma parameters such as density, temperature, and elemental abundances are derived by reference to atomic data base like CHIANTI (Dere et al. 1997; Del Zanna et al. 2015). Figure 6.4(a) shows the density range covered by suitable density-sensitive line ratios available to Solar-C_EUVST as a function of the line formation temperature, whereas Figure 6.4(b) shows the temperature range covered by suitable temperature-sensitive line ratios available to Solar-C_EUVST as a function of the line formation temperature. Non-thermal velocities are determined by subtracting the thermal and instrumental widths from the observed line width. Doppler velocities in the long wavelength channels are generally measured relative to emission lines from neutral atoms, which are assumed to be at rest. In the short channel, Doppler velocities are measured relative to the quiet Sun and have larger uncertainties.

Comparisons with simultaneous photospheric and low-chromospheric measurements obtained by other space-borne and ground-based observatories (e.g., magnetograms by SDO/HMI and DKIST) are essential for revealing the relationship between the atmospheric dynamics and surface evolutions. Furthermore, various kinds of state-of-the-art numerical simulations support the interpretation of observational results. The proposed scientific objectives will be achieved through the balanced combination of the different methods mentioned above.

Data analysis tools, including the software for data prepping and fitting Gaussian line profiles, will be provided by the Solar-C_EUVST science team. Observational data will be publicly available soon after initial calibrations are made. Online search tools that help users locate data will also be provided.

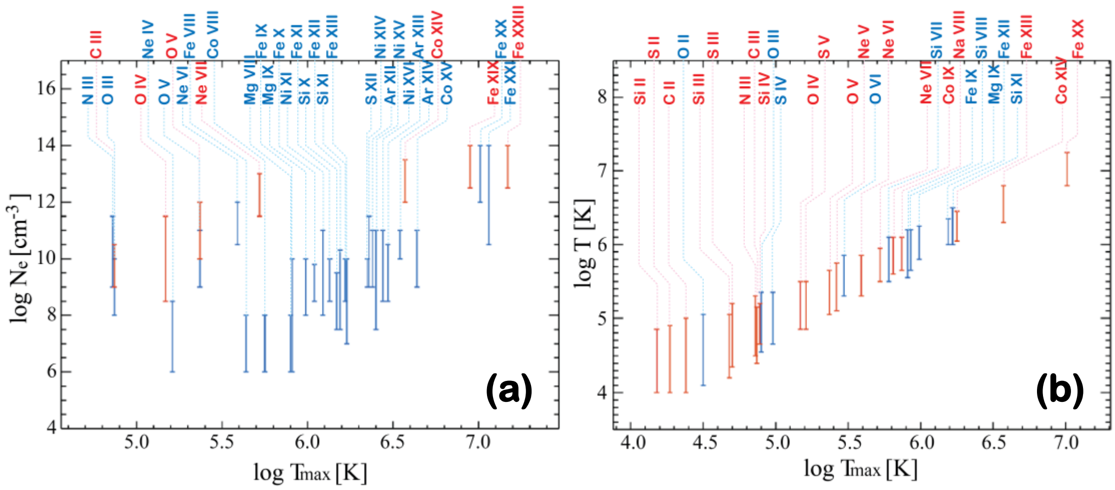

Figure 6.4: (a) Electron density range covered by the density-sensitive intensity line ratios available in the Solar-C_EUVST spectral bands as a function of the formation temperature of the line pair. Densities obtained from ratios with all components on the same channel are shown in blue while those having components on different channels are shown in red. (b) Electron temperature range covered by the temperature-sensitive intensity line ratios available in the Solar-C_EUVST spectral bands as a function of the formation temperature of the line pair. The best diagnostics (bright or relatively bright lines and good temperature coverage) are shown in blue. Density and temperature ranges are evaluated with CHIANTI 7.1.

7. Scientific traceability matrix (draft) [1-4-1]
科学トレーサビリティマトリックス

The science requirements traceability matrix (Table 7.1) shows the breakdown flow from science objectives to key instrument and mission data requirements. The driving requirement for investigations (third column from the left) is based on Tables 5.1 to 5.6. If one sub-objective proposes multiple observing tasks, we show the most demanding values for the driving requirement. These driving requirements are then translated into a set of instrument requirements (second column from the right) in the following manner. Broad temperature coverage in bright emission lines directly determines the wavelength requirement. The effective area is derived from the required spatial resolution, temporal resolution, and count rates; the count rates here are determined so as to meet the velocity (Doppler and width) resolution requirements. These calculations include a combined spectral width of 2.5 pixels, which considers the slit width and instrumental broadening (see section 6.2.4). However, the sensitivity study using a combined spectral width of 3.0 pixels show only a minimal (~20%) increase in the required amount of counts. Therefore, 2.0 pixels were adopted as the spectral resolution requirement. We defined the effective area for each wavelength band (SW, LW1, LW2, LW3) as the area necessary to obtain 200 counts per exposure. Here, the value of 200 comes from the requested velocity resolution (e.g., 2 km/s) in the driving requirement for investigations (third column from the left), while the exposure time is based on the temporal resolution in the same column. We calculated the count rates for the typical emission line of each wavelength band, i.e., Fe XII (SW: 195 Å), Ne VIII (LW1: 770 Å), Fe XVIII (LW2: 975 Å), and C III (LW3: 1176 Å). Observing program requirements determine the FOV- and raster-related requirements. Data and compression requirements as well as downlink capabilities are directly driven by the characteristics of the observing program. Co-registration of the slit position is needed to analyze the observations in conjunction with other data sets.

Table 7.1: Scientific traceability matrix

Science Goal
Understand how the plasma universe is created and evolves, and how the Sun influences the Earth and other planets in our solar system

Science Objective I
Understand how fundamental processes lead to the formation of the solar atmosphere and the solar wind

Sub-objectives	Investigations: Physical parameters: Observing Tasks	Investigations: Physical parameters: Driving Requirement [High cadence obs.]	Investigations: Observables	Instruments: Design Parameters	Instruments: Requirement [High cadence obs.]	Mission data requirements
I-1: Quantify the Contribution of Nanoflares to Coronal Heating	Energy of small-scale heating events in the corona with energies down to 10^{24} erg	Te coverage: 0.8-10 MK	UV/EUV Emission-line profiles (intensity, velocity, width, spectral shape), with formation temperature (0.8-10 MK)	Wave length:	SW, LW2	3500 s / 2.52 Gb 0.72 Mbps
		Target Spatial Scale: 0.4"		Spatial Resolution:	0.4"	
		Temporal resolution: 5s/0.4"		Effective area (cm^2):	SW: >0.7, LW1: >0.5, LW2: > 2.8, LW3: >0.3	
		Target size: 280”×280"		FOV:	0.4"×100"	
		Velocity resolution: Vd~2km/s, Vnt~5km/s		Spectral resolution λ/Δλ:	SW:5000, LW:13500	
		Observation duration: 1 hour		Cadence of area coverage:	5s	
	Hot (5 MK) fast flow in FeXVIII associated with nanoflare	Te coverage: 0.8-10 MK	UV/EUV Emission-line profiles (intensity, velocity, width, spectral shape), with formation temperature (0.8-10 MK)	Wave length:	SW, LW2	3500 s / 2.52 Gb 0.72 Mbps
		Target Spatial Scale: 0.4"		Spatial Resolution:	0.8	
		Temporal resolution: 1.5s/0.8"		Effective area (cm^2):	SW: >0.5, LW1: >0.4, LW2: > 2, LW3: >0.2	
		Target size: 280"×280"		FOV:	0.8"×280"	
		Velocity resolution: Vd~2km/s, Vnt~5km/s		Spectral resolution λ/Δλ:	SW:5000, LW:13500	
		Observation duration: 1 hour		Cadence of area coverage	1.5s	
	Sub-arcsec braiding structures	Te coverage: 0.8-10 MK	UV/EUV Emission-line profiles (intensity, velocity, width, spectral shape), with formation temperature (0.8-10 MK)	Wave length:	SW, LW2	3200 s / 1.92 Gb 0.60 Mbps
		Target Spatial Scale: 0.4”		Spatial Resolution:	0.4" [0.8"]	
		Temporal resolution: 5sec/0.4" [1.5s/0.8"]		Effective area (cm^2):	SW: >0.7, LW1: >0.5, LW2: > 2.8, LW3: >0.3	
		Target size: 280"×280"		FOV:	20"×100" [20"×280"]	
		Velocity resolution: Vd~2km/s, Vnt~5km/s		Spectral resolution λ/Δλ:	SW:5000, LW:13500	
		Observation duration: 1 hour		Cadence of area coverage	250s [37.5s]	
I-2: Quantify the Contribution of Wave Dissipation to Coronal Heating	Velocity fluctuations of Alfvén wave (Doppler and line width) through different layers of the atmosphere	Te coverage: 0.02-3 MK	UV/EUV Emission-line profiles (intensity, velocity, width, spectral shape), with formation temperature (0.02-3 MK)	Wave length:	SW, LW1, LW2, LW2 (2nd), LW3	3500 s / 4.12 Gb 1.18 Mbp s
		Target Spatial Scale: 0.4"		Spatial Resolution:	0.4" [1.6"]	
		Temporal resolution: 2s/0.4" [0.5s/1.6"]		Effective area (cm^2):	SW: >1.4, LW1: >1, LW2: > 5.6, LW3: >0.6	
		Target size: 280"×280"		FOV:	10"×100" [280"×280"]	
		Velocity resolution: Vd~2km/s		Spectral resolution λ/Δλ:	SW:5000, LW:13500	
		Observation duration: 1 hour		Cadence of area coverage	50s [87.5s]	
	Temporal variation of coronal density, velocity, temperature associated with waves propagation	Te coverage: 0.02-3 MK	UV/EUV Emission-line profiles (intensity, velocity, width, spectral shape), with formation temperature (0.02-3 MK)	Wave length:	SW, LW1, LW2, LW2 (2nd), LW3	3500 s / 2.52 Gb 0.72 Mbps
		Target Spatial Scale: 0.4"		Spatial Resolution:	0.4" [1.6"]	
		Temporal resolution: 2s/0.4" [0.5s/1.6"]		Effective area (cm^2):	SW: >1.4, LW1: >1, LW2: > 5.6, LW3: >0.6	
		Target size: 280"×280"		FOV:	10"×100" [280"×280"]	
		Velocity resolution: Vd~2km/s		Spectral resolution λ/Δλ:	SW:5000, LW:13500	
		Observation duration: 1 hour		Cadence of area coverage:	50s [87.5s]	
I-3: Understand the Formation Mechanism of Spicules and Quantify Their Contribution to Coronal Heating	Temporal variation of density, velocity, temperature of spicules and coronal plasma	Te coverage: 0.02-3 MK	UV/EUV Emission-line profiles (intensity, velocity, width, spectral shape), with formation temperature (0.02-3 MK)	Wave length:	SW, LW1, LW2, LW2 (2nd), LW3	3000 s / 2.18 Gb 0.72 Mbps
		Target Spatial Scale: 0.4"		Spatial Resolution:	0.4"	
		Temporal resolution: 2s/0.4"		Effective area (cm^2):	SW: >1.4, LW1: >1, LW2: > 5.6, LW3: >0.6	
		Target size: 5"×50"		FOV:	10"×100"	
		Velocity resolution: Vd~2km/s		Spectral resolution λ/Δλ:	SW:5000, LW:13500	
		Observation duration: 1 hour		Cadence of area coverage:	50s	
I-4: Understand the Source Regions and the Acceleration Mechanism of the Solar Wind	Velocity, temperature, density, and their fluctuations in the source of solar wind region	Te coverage: 0.7-3 MK	UV/EUV Emission-line profiles (intensity, velocity, width, spectral shape), with formation temperature (0.7-3 MK)	Wave length:	SW, LW2 (2nd)	3400 s / 2.19 Gb 0.64 Mbps
		Target Spatial Scale: 0.4"		Spatial Resolution:	0.8"	
		Temporal resolution: 1.5s/0.8"		Effective area (cm^2):	SW: >0.5, LW1: >0.4, LW2: > 2, LW3: >0.2	
		Target size: 280"×280"		FOV:	280"×280"	
		Velocity resolution: Vd~2km/s, Vnt~5km/s		Spectral resolution λ/Δλ:	SW:5000, LW:13500	
		Observation duration: 1 hour		Cadence of area coverage:	525s	
	Height dependence of energy flux of Alfven wave in plume and inter-plume regions	Te coverage: 0.7-3 MK	UV/EUV Emission-line profiles (intensity, velocity, width, spectral shape), with formation temperature (0.7-3 MK)	Wave length:	SW, LW2 (2nd)	3500 s / 0.54 Gb 0.15 Mbps
		Target Spatial Scale: 10"		Spatial Resolution:	0.8"	
		Temporal resolution: 5min/0.8"		Effective area (cm^2):	SW: >1.5, LW1: >1.2, LW2: n/a, LW3: >0.6	
		Target size: 10"×1000"		FOV:	0.8"×280"	
		Velocity resolution: Vd~2km/s, Vnt~4km/s		Spectral resolution λ/Δλ:	SW:5000, LW:13500	
		Observation duration: 1 hour		Cadence of area coverage	5min	

Table 7.1: Scientific traceability matrix (continue)

Science Objective II
Understand how the solar atmosphere becomes unstable, releasing the energy that drives solar flares and eruptions

Sub-objectives	Investigations: Physical parameters: Observing Tasks	Investigations: Physical parameters: Driving Requirement [Fast cadence obs.]	Investigations: Observables	Instruments: Design Parameters	Instruments: Requirement [Fast cadence]	Mission data requirements
II-1: Understand the Fast Magnetic Reconnection Process	Velocity, temperature, density, and ionization state in the reconnection region	Te coverage: 0.8-15 MK	UV/EUV Emission-line profiles (intensity, velocity, width, spectral shape), with formation temperature (0.8-15 MK)	Wave length:	SW, LW3 (2nd)	2 days / 322 Gb 1.87 Mbps
		Target Spatial Scale: 3"		Spatial Resolution:	0.8"	
		Temporal resolution: 0.5s/0.8"		Effective area (cm^2):	SW: >0.5, LW1: >0.3, LW2: > 0.5, LW3: >0.3	
		Target size: 5"×20"		FOV:	20"×280"	
		Velocity resolution: Vd~2km/s		Spectral resolution $\lambda/\Delta\lambda$:	SW:5000, LW:13500	
		Observation duration: a few days		Cadence of area coverage:	12.5s	
	Velocity, temperature, and density in the chromospheric evaporation	Te coverage: 0.02-15 MK	UV/EUV Emission-line profiles (intensity, velocity, width, spectral shape), with formation temperature (0.02-15 MK)	Wave length:	SW, LW1, LW2, LW2 (2nd), LW3, LW3 (2nd)	2 days / 322 Gb 1.87 Mbps
		Target Spatial Scale: 1"		Spatial Resolution:	0.8"	
		Temporal resolution: 0.5s/0.8"		Effective area (cm^2):	SW: >0.5, LW1: >0.3, LW2: > 0.5,LW3: >0.3	
		Target size: 1"×50"		FOV:	0.8"×280"	
		Velocity resolution: Vd~2km/s		Spectral resolution $\lambda/\Delta\lambda$:	SW:5000, LW:13500	
		Observation duration: a few days		Cadence of area coverage	0.5s	
	Velocity, temperature, density, and ionization state in the chromospheric reconnection region	Te coverage: 0.02-3 MK	UV/EUV Emission-line profiles (intensity, velocity, width, spectral shape), with formation temperature (0.02-3 MK)	Wave length:	SW, LW1, LW2, LW2 (2nd), LW3	3200 s / 2.08 Gb 0.66 Mbps
		Target Spatial Scale: 0.4"		Spatial Resolution:	0.8"	
		Temporal resolution: 1.5s/0.8"		Effective area (cm^2):	SW: >0.5, LW1: >0.4, LW2: > 2, LW3: >0.2	
		Target size: 1"x10"		FOV:	20"×280"	
		Velocity resolution: Vd~2km/s		Spectral resolution $\lambda/\Delta\lambda$:	SW:5000, LW:13500	
		Observation duration: a few days		Cadence of area coverage	37.5s	
II-2: Identify the Signatures of Global Energy Buildup and the Local Triggering of the Flare and Eruption	Long term evolution of velocity, temperature, density, and turbulence energy in active regions	Te coverage: 0.02-10 MK	UV/EUV Emission-line profiles (intensity, velocity, width, spectral shape), with formation temperature (0.02-10 MK)	Wave length:	SW, LW1, LW2, LW2(2nd), LW3	1 week / 36.96 Gb 0.06 Mbps
		Target Spatial Scale: 10"		Spatial Resolution:	0.8"	
		Temporal resolution: 1.5s/0.8"		Effective area (cm^2):	SW: >0.5, LW1: >0.4, LW2: > 2, LW3: >0.2	
		Target size: 280"×280"		FOV:	280"×280"	
		Velocity resolution: Vd~2km/s, Vnt~5km/s		Spectral resolution $\lambda/\Delta\lambda$:	SW:5000, LW:13500	
		Observation duration: a few days		Cadence of area coverage	525s	
	Velocity, temperature, and density in the flare triggering regions	Te coverage: 0.02-1 MK	UV/EUV Emission-line profiles (intensity, velocity, width, spectral shape), with formation temperature (0.02-1 MK)	Wave length:	SW, LW1, LW2, LW2 (2nd), LW3	2 days / 111 Gb 0.64 Mbps
		Target Spatial Scale: 10"		Spatial Resolution:	0.8"	
		Temporal resolution: 1.5s/0.8"		Effective area (cm^2):	SW: >0.5, LW1: >0.4, LW2: > 2, LW3: >0.2	
		Target size: 20"×20"		FOV:	20"×280"	
		Velocity resolution: Vd~2km/s		Spectral resolution $\lambda/\Delta\lambda$:	SW:5000, LW:13500	
		Observation duration: a few days		Cadence of area coverage	12.5s	

1) 1": 730 km, V_d: Doppler velocity, V_{nt}: nonthermal velocity (e.g., turbulence)
2) Coregistration of the slit position with solar features of <0.18".
3) Required spectral resolution corresponds to a two pixel average FWHM over the central 100" of each detector.